International Journal of Pharmaceutics 640 (2023) 122977

Contents lists available at ScienceDirect

International Journal of Pharmaceutics

journal homepage: www.elsevier.com/locate/ijpharm

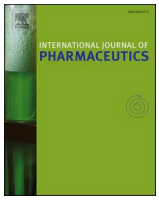

Enhanced *in vitro* and *in vivo* anticancer activity through the development of Sunitinib-Loaded nanoniosomes with controlled release and improved uptake

Shiva Dehghan [a], Amirhossein Naghipour [b], Fatemeh Zomorodi Anbaji [c], Pezhman Golshanrad [d], Hosein Mirazi [e], Hossein Adelnia [f], Mahdi Bodaghi [g,*], Bahareh Farasati Far [h,*]

[a] School of Pharmacy, Shiraz University of Medical Sciences, Shiraz, Iran
[b] Department of Pharmaceutics, Faculty of Pharmacy, Kerman University of Medical Sciences, Kerman, Iran
[c] Department of Cell &Molecular Biology, School of Biology, College of Science, University of Tehran, Tehran, Iran
[d] Department of Computer Engineering, Sharif University of Science and Technology (International Campus), Tehran, Iran
[e] Tissue engineering, Faculty of New Science and Technology, University of Tehran, Tehran, Iran
[f] Australian Institute for Bioengineering and Nanotechnology, The University of Queensland, Brisbane, QLD 4072, Australia
[g] Department of Engineering, School of Science and Technology, Nottingham Trent University, Nottingham, NG11 8NS, UK
[h] Department of Chemistry, Iran University of Science and Technology, Tehran, Iran

ARTICLE INFO

Keywords:
Lung cancer
Chemotherapy, nanoniosome
Sunitinib
Drug delivery system
Collagen
Protein-coating

ABSTRACT

This study aims to develop sunitinib niosomal formulations and assess their *in-vitro* anti-cancer efficiency against lung cancer cell line, A549. Sunitinib, a highly effective anticancer drug, was loaded in the niosome with high encapsulation efficiency. Collagen was coated on the surface of the niosome for enhanced cellular uptake and prolonged circulation time. Different formulations were produced, while response surface methodology was utilized to optimize the formulations. The stability of the formulations was evaluated over a 2-month period, revealing the importance of collagen coating. MTT assay demonstrated dose-dependent cytotoxicity for all formulations against lung cancer cells. Scratch assay test suggested antiproliferative efficacy of the formulations. The flow cytometry data confirmed the improved cytotoxicity with enhanced apoptosis rate when different formulations used. The 2D fluorescent images proved the presence of drug-containing niosomes in the tumor cells. The activation of the apoptotic pathway leading to protein synthesis was confirmed using an ELISA assay, which specifically evaluated the presence of *cas3* and *cas7*. The results of this study indicated the antiproliferative efficacy of optimized niosomal formulations and their mechanism of action. Therefore, niosomes could be utilized as a suitable carrier for delivering sunitinib into lung cancer cells, paving the way for future clinical studies.

1. Introduction

Lung cancer accounts for the highest mortality rate among men and women worldwide (Siegel et al., 2014). It has been estimated that 85 to 90% of all lung cancer cases are caused by non-small cell lung cancer (NSCLC), while the remaining 10% are caused by small cell lung cancer (Molina et al., 2008). The main treatment option for NSCLC patients is chemotherapy, which is inoperable in 85% of cases (Provencio et al., 2011). A 5-year survival rate of 1–14 % was observed for patients treated with traditional cytotoxic chemotherapy at advanced stages of NSCLC (Farasati Far et al., 2022b; Wang et al., 2010). Traditional chemotherapy drugs lack target specificity, which has led to molecularly targeted therapies (Stella et al., 2012).

Niosomes are composed of an aqueous core, and a lipid bilayer comprising nonionic surfactants and cholesterol (as lipids). Employing such structure, one could load both hydrophilic and hydrophobic agents, the former in the aqueous core, and the latter in the lipid bilayer. By formulating the biocompatible ingredient in the design of niosomes, they could be even more biocompatible than other conventional nanocarriers. The niosomal formulation can be devised in a way to develop stimuli-responsive carriers, such as pH-sensitive niosomes that burst under acidic conditions. Such sensitivity is of great interest in cancer

* Corresponding authors.
E-mail addresses: mahdi.bodaghi@ntu.ac.uk (M. Bodaghi), farasatifar_bahareh@cmps2.iust.ac.ir (B.F. Far).

https://doi.org/10.1016/j.ijpharm.2023.122977
Received 9 February 2023; Received in revised form 1 April 2023; Accepted 18 April 2023
Available online 29 April 2023

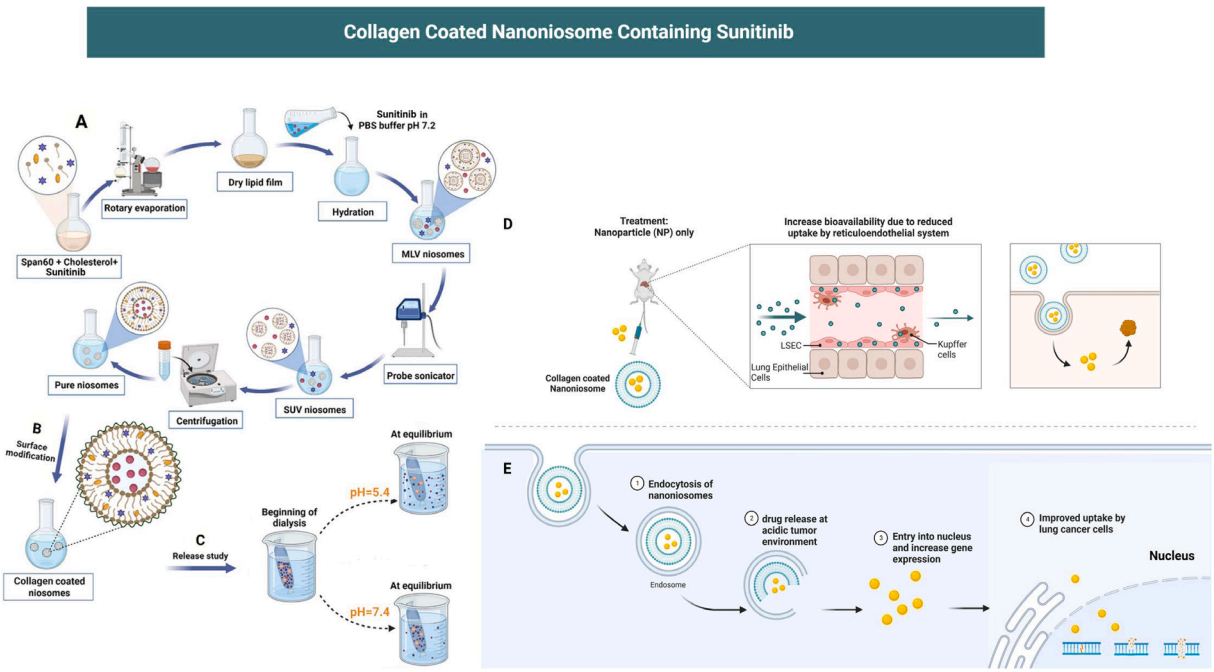

Scheme 1. Schematic presentation of collagen coated nanoniosome containing sunitinib. (A) Preparation and (B) surface modification of nanoniosomes by thin-layer hydration method. (C) *in vitro* drug release under various pH conditions (5.4 and 7.4), (D) Improvement of sunitinib bioavailability by collagen coating, (E) Improve uptake of lung cancer cells through encapsulation by niosome. SUV: small unilamellar niosomes; MLV: multilamellar niosomes.

Table 1
Vesicle size, EE%, and PDI of Different Niosomal Formulations Containing sunitinib. Data are represented as Mean ± SD, n = 3.

		Factor 1	Factor 2	Factor 3	Response 1	Response 2	Response 3
Std[1]	Run	Drug content	Surfactant: Cholesterol	Lipid: Drug	Size	EE	Release (PBS 7.4)
	unit	mg	molar ratio	molar ratio	nm	%	%
8	1	15	1	30	328.302	99.0247	65.1022
12	2	10	2	30	345.969	95.5725	58.9478
7	3	5	1	30	243.945	95.933	58.9086
6	4	15	1	10	201.474	98.4771	67.905
5	5	5	1	10	191.178	88.1462	49.6966
4	6	15	2	20	287.182	92.5855	58.1834
1	7	5	0.5	20	357.552	88.9908	42.4642
14	8	10	1	20	218.439	96.7046	61.29
3	9	5	2	20	261.963	91.9263	46.933
10	10	10	2	10	232.479	86.0553	52.47
13	11	10	1	20	223.821	97.478	60.2806
2	12	15	0.5	20	376.857	91.5555	54.822
11	13	10	0.5	30	409.328	93.8936	59.673
9	14	10	0.5	10	318.847	81.7087	52.1956
15	15	10	1	20	219.141	97.9209	63.495

[1] Standard order.

targeting therapy, as the cancerous microenvironment has been proved acidic due to oversecretion of lactic acid by aerobic glycolysis. Additionally, it has been shown that several cancer types, including NSCLC, overexpress epidermal growth factor receptors (EGFRs) (Alharbi et al., 2022). Using these properties, one could significantly enhance the delivery and release of drugs with the least side effects (Garg et al., 2022).

The inherent attachment of some types of proteins to the surface of niosomes has proven to be highly effective in developing targeted drug-loaded therapeutic agents (Honarvari et al., 2022; Karooby and Granpayeh, 2019). Additionally, it is widely known that adding certain molecules to the niosome membrane can modify their *in vivo* activity, rendering niosomes highly flexible and effective in therapeutics efficiency (Torchilin, 2005). Lipid exchange with high-density lipoproteins (HDL) leads to niosome breakdown and peroxidation, followed by macrophage absorption and the fast clearance of niosomes from the bloodstream (Pradhan et al., 2018). Nonetheless, it has been shown that the presence of cholesterol, gangliosides, poly(ethylene glycol) (PEG), protein like collagen (Extracellular matrix protein), and polysaccharides like chitosan can effectively decrease the rates of these interactions, prolonging the niosome circulating time (Shi et al., 2021).

It has been shown that PEGs or gangliosides extend their half-life by creating a super hydrophilic layer on the niosome surface, preventing the binding of unspecific plasma proteins. In addition, such species on the niosome surface reduce electrostatic charges, thereby preventing this kind of interaction (Fu et al., 2021).

Sunitinib malate (SUNI) inhibits multiple tyrosine kinases and shows strong antitumor and antiangiogenic properties (Escudero-Ortiz et al., 2022). Various (pre)clinical studies have shown that SUNI is effective against a variety of solid tumors such as breast, colon, neuroendocrine, and lung (Vázquez et al., 2021). SUNI has been studied in conjunction with imatinib to treat advanced renal cell carcinoma, progression-resistant gastrointestinal stromal tumors, and well-differentiated

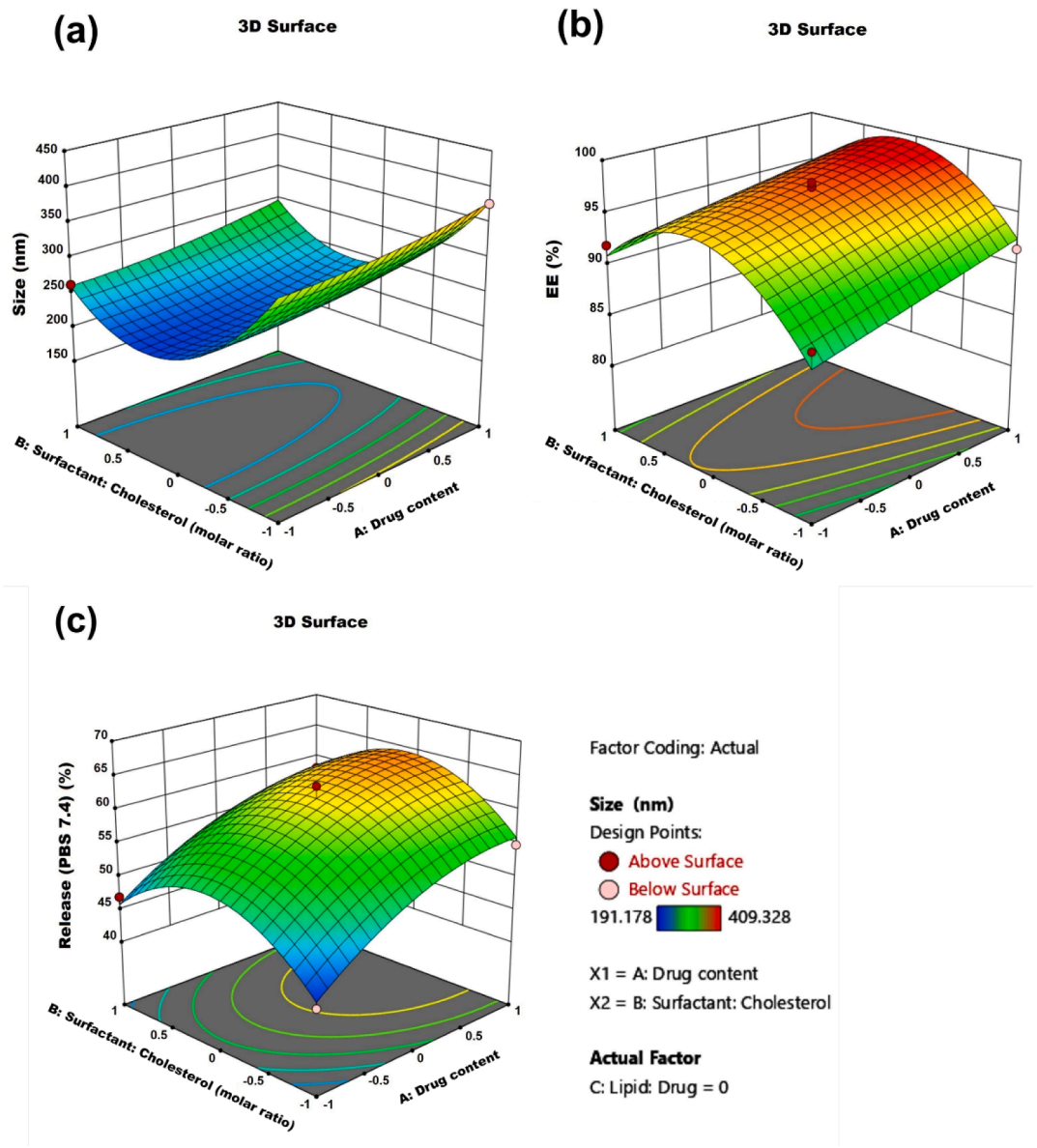

Fig. 1. Three-dimensional response surface plots of Niosomal Formulations for A) size, B) EE, and C) EE as a function of the parameters (lipid concentration and surfactant/cholesterol ratio).

neuroendocrine tumors of the pancreas (Westerdijk et al., 2021). Sunitinib is a multitargeted inhibitor of several tyrosine kinase receptors, including VEGF, PDGF, and c-KIT, among others. Its anti-angiogenic effects are primarily attributed to its ability to block the VEGF receptor, thereby inhibiting the formation of new blood vessels for tumor growth and metastasis. Additionally, sunitinib can also inhibit the proliferation of lung cancer cells by targeting other tyrosine kinase receptors, such as PDGF and c-KIT, which are involved in cancer cell survival and growth. These anti-angiogenic and anti-proliferative effects of sunitinib make it a promising candidate for the treatment of lung cancer. This disease is often characterized by an increase in angiogenesis, which could be disrupted by the sunitinib's ability through blocking the VEGF receptor signaling. Furthermore, sunitinib has shown promising results in clinical trials for the treatment of advanced non-small cell lung cancer, which is the most common type of lung cancer (Wang and Tang, 2023). In addition, sunitinib showed clinical activity against NSCLC. In animal and human studies, the pharmacokinetic profile of sunitinib is well documented (Speed et al., 2012). Sunitinib concentrations in cancer patients have been reported to be 20–30 ng/ml and to achieve maximum plasma levels within 5–7 h (Malnoë et al., 2022). *In vivo* bioavailability of sunitinib is limited because of its poor water solubility. Therefore, loading SUNI into niosome may enhance its solubility, bioavailability, and local anti-tumor efficacy while reducing the systemic toxicity.

In light of the above-mentioned, the present work aims to prepare SUNI-loaded niosomes coated with collagen and investigate their *in vitro* activity in combating lung cancer cells, see Scheme 1. Therefore, we investigated the feasibility of employing a closely associated protein (collagen) to achieve a similar steric effect. To combat advanced lung cancer cases, this study created and characterized the physicochemical properties of drug-loaded nanoniosomes with a collagen coating. Nanoniosomes loaded with drugs are less toxic because their collagen coating facilitates endocytosis into cells. Over this, it can potentially be an effective drug delivery system for treating lung cancer. In this study, we report the new strategy of adding hydrophobically derivatized collagen to the surface of the niosome to increase its stability and

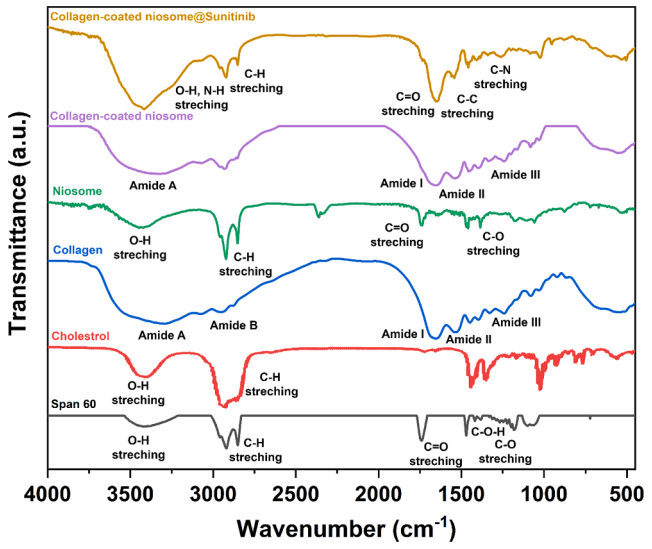

Fig. 2. FTIR spectra of samples and the ingredients used in the preparation of formulations. The spectra show that nanoniosomes has been successfully synthesized.

biodistribution, thereby enhancing cellular absorption and inducing more apoptosis via the sunitinib anticancer drug.

2. Materials and methods

2.1. Materials

Chloroform, ethanol, Span 60, dimethyl sulfoxide (DMSO), cholesterol, ultra-15 membrane (Amicon, MWCO 30,000 Da), and 1,2-stearoyl-*sn*-glycerol-3-phosphoethanolamine-N-[folate(polyethylene glycol)-2000] (ammonium salt) were supplied from Merck, Germany. RPMI-1640 medium, trypsin-EDTA, trypan blue, DMEM, PBS, fetal bovine serum (FBS), on 3-(4,5-Dimethylthiazol-2-yl)-2,5-diphenyltetrazolium bromide (MTT), and penicillin/streptomycin 100x (P/S) were all acquired from Gibco, USA. Collagen (Type II) and a dialysis membrane (MWCO 12000 Da) were purchased from Sigma, USA. A549 cell line was also received from Iran's Pasteur Cell Bank. Sunitinib Maleate was supplied from Selleck USA. The apoptosis detection kit consisting of an annexin V/propidium iodide (PI) assay was supplied from Roche, Germany. The necessary RNA extraction kit was received from Qiagen, USA. The cDNA was synthesized with a Revert AidTM First Strand cDNA Synthesis Kit (Fermentas, Vilnius, Lithuania).

2.2. Preparation of Sunitinib-Loaded niosomes

To develop sunitinib-loaded niosomes, a modified version of a thin-layer hydration approach which was described in our earlier design was used (Sahrayi et al., 2021). Sunitinib (10 mg), cholesterol (38 mg), and span60 (57 mg) were all dissolved in chloroform (9 mL) and then evaporated in a rotary evaporator (150 rpm, 60 °C, 40 min). PBS (1x) pH 7.4 was used to rehydrate the dried thin films at 25 °C (130 rpm, 30 min). After centrifugation (10000 rpm, 10 min), the obtained sunitinib-loaded niosomes were redispersed by sonicating the pellet for 5 min (10000 rpm, 10 min) with a consistent size distribution were obtained by probe sonicating (300 Hz) the sample for 10 min. The samples were stored in at 4 °C for further experiments. By omitting sunitinib from the formulation, pure (drug free) niosomes were also prepared. For modification of niosome by collagen, a 2% (w/w) of collagen in PBS was prepared to which the niosome dispersion (10 mg/mL) was added dropwise under stirring conditions.

2.3. Entrapment efficiency

Using an Amicon Ultra-15 membrane, the solution containing the drug-loaded niosomes was ultra-filtered at 4000 *x*g for 20 min (MWCO 30,000 Da). After placing 500 μL of the formulation in the cell's inner chamber, the assembly was centrifuged for 20 min at 4000 *x*g at 4 °C. While the drug-loaded niosomes remained in the top compartment, the accessible drug (i.e., unloaded) passed through the filter. UV–visible spectrophotometry at 423 nm was used to calculate the free drug concentration in the device's outer chamber (JASCO, V-530, Japan). The following formulae were used to determine the encapsulation efficiency (EE) and loading efficiency (LE). The following standard curve plotted in Figure S1 was utilized to calculate drug concentration. The EE was then calculated by the following Eq. (1):

$$\text{Encapsulation Efficiency}\,(\%) = \left[\frac{\text{Initial drug loaded} - \text{Free Drug}}{\text{Initial drug loaded}}\right] \times 100 \quad (1)$$

2.4. In vitro drug release study and kinetic models

10 mL of each drug-encapsulated nanoniosome sample was placed in a dialysis bag (MWCO = 12 kDa) for the *in-vitro* drug release analysis. PBS solution (50 mL, 1x, pH = 5, and 7.4) was used as the release media, and the solution was then stirred slowly (50 rpm) at 37 °C. At certain intervals, the PBS solution was discarded and replaced with new aliquots. The amount of drug released was calculated using the standard curve equation mentioned above.

The release profile was examined using Higuchi, Korsmeyer-Peppas, zero-order, and first-order release kinetic models. In these models, the percentage of drug released is plotted against the square root of time, the logarithm of time, and time itself, respectively. In the first-order model, however, the released drug is plotted against the percentage of the drug still in the system. The linear curve was determined using the regression values of the correlation coefficient (r) from the plots generated by the aforementioned models.

Dialysis bags have been used in the same release experiment containing drug powder with comparable initial drug concentrations.

2.5. Instrumental characterization

Zeta-sizer equipment (Model Nano ZS3600, Malvern, UK) was used to measure the niosomes' average hydrodynamic particle size, particle distribution index (PDI), and zeta potential at 25 °C. The absorbance of the samples was measured with a UV–Vis spectrophotometer (Shimadzu UV-1700 Pharma spec, Japan). The surface morphology of the formulations was studied by field emission scanning electron microscopy (FESEM), transition electron microscopy (TEM), and atomic force microscopy (AFM). For FESEM, a drop of the SUNI@Nio/Col dispersion was placed on a silicon wafer and dried in a desiccator overnight. A thin layer of gold was then sputtered onto the samples, and the coated samples were analyzed by a field emission scanning electron microscope (FESEM) (NOVA NANOSEM 450 FEI, USA). For TEM, a drop of the formulation was placed on carbon-coated, 300-mesh copper grids, and the excess sample was filtered off after 2 min with paper towels. Distilled water was used as the eluent, while Uranyl acetate was used as the stain of TEM samples at a concentration of 2%. A field emission TEM (TENAI G2 F20, USA) was used at an acceleration voltage of 80 kV. To prepare samples for AFM, 10 μL of diluted (1:20) dispersion of the formulations were spread out on 1 cm^2 of glass slides and allowed to dry at room temperature. The samples were viewed in an AFM equipped with a Nanowizard II (JPK Instruments, Berlin, Germany) and low-stress silicon nitride cantilevers (AppNano, USA) operating in AC mode at 66 k Hz scan.

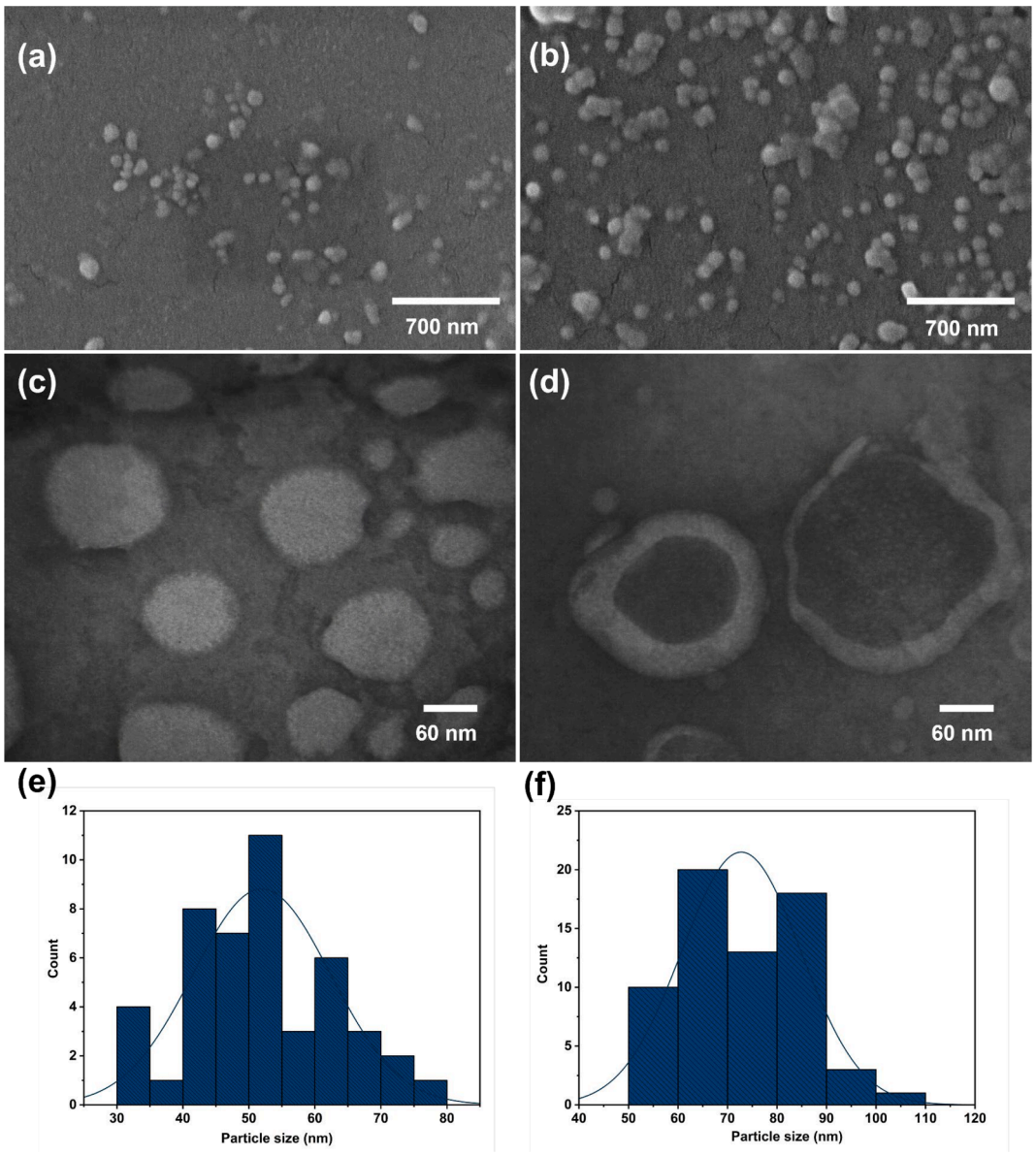

Fig. 3. FESEM images of (a) SUNI@Nio and (b) SUNI@Nio/Col, TEM images of (c) SUNI@Nio and (d) SUNI@Nio/Col, and Size distribution histogram of (e) SUNI@Nio and (f) SUNI@Nio/Col designed by ImageJ.

2.6. Stability studies

SUNI@Nio and SUNI@Nio/Col were tested for 60 days at 25 °C and 4 °C. The average hydrodynamic size (defined as Z-average), PDI, and EE of the dispersions were measured on days 15, 30, and 60 since the synthesis date and compared with the results obtained immediately after the synthesis. It is of noteworthy that that the samples were kept undisturbed (without any shaking or mixing) during the stability test, which is different from the release study conditions. Therefore, less release is expected to be seen during the stability test.

2.7. Cytotoxicity assay

Using a colorimetric technique based on MTT, cytotoxicity of the prepared samples was determined in human lung cancer cell lines (A549). Briefly, cells were grown in RPMI-1640 (containing 1% P/S and 10% FBS; 5×10^5 cells/well in a 96 well plate) and incubated at 37° C for 24 h in a 5% carbon dioxide atmosphere. The cell lines were then exposed to various sample concentrations of the formulations for 48 h before being analyzed. After 48 h of incubation at T = 37 °C in a 5% CO_2 environment, the medium in each well was changed out for MTT (20 μL, 5 mg/mL). Formazan crystals produced by the living cells were dissolved by adding 100 L of isopropanol to the remaining supernatant. Finally, the absorbance at 570 nm was recorded using an ELISA Reader (Organon Teknika, Oss, Netherlands) to determine cytotoxicity by comparing treated cells to untreated cells in the control group. Sunitinib and empty nanoniosomes as the positive and negative controls, respectively.

To ensure the sterility of our nanoniosomes, The prepared formulations were filtered using a 0.22 μm syringe filter prior to each experiment. This method of sterilization is commonly used in nanotechnology and has been shown to effectively remove any potential bacterial or fungal contaminants.

2.8. Flow cytometry

A549 cells were seeded at a density of 5 × 105 cells/well in 6-well plates and then incubated overnight at 37 °C in 5% CO2 to ensure

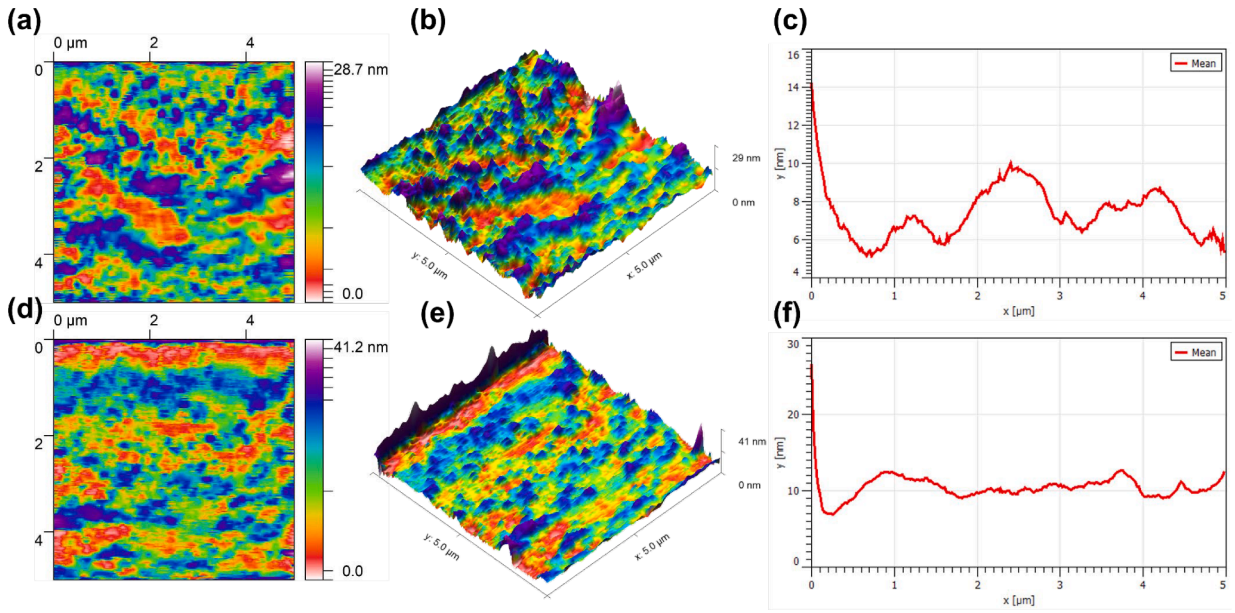

Fig. 4. AFM images (a) 2D image of SUNI@Nio, (b) 3D images of SUNI@Nio, and (c) Size distribution flowchart of SUNI@Nio, (d) 2D image of SUNI@Nio/Col, (e) 3D images of SUNI@Nio/Col, and (f) Size distribution flowchart of SUNI@Nio/Col.

complete attachment before the apoptosis/necrosis ratio could be determined. Then, the cells were incubated for 48 h with the prepared formulation at the IC50 concentration obtained above. After 48 h, the cells were washed using sterile PBS (pH 7.4) and suspended in 1X binding buffer supplied by the kit (Transgene Biotech ER101-01), and the cells were investigated using Annexin V/propidium iodide (PI) test. As a comparison, untreated A549 cells served as the standard. At last, flow cytometry analysis was used to measure the percentage of dead and live cells (FACSCalibur, BD Biosciences, Singapore).

2.9. Apoptotic gene expression analysis

SUNI@Nio and SUNI@Nio/Col were used to treat A549 cells for 24 h at the IC_{50} concentrations. To isolate the RNA content of the treated cells, the RNA extraction kit (Transgene Biotech) was used. The cDNAs were extracted using the cDNA synthesis kit (Takara, Japan). The expression levels of *Bax*, *CDKN2A*, *B2M*, *Caspase 8 (Cas8)*, and *Caspase 9 (Cas9)* was analyzed by real-time PCR with *B2M* as the housekeeping gene for the reference point. Table S1 contains the primers utilized for real-time PCR. Real-time PCR was carried out at 95 °C-10 min, 95 °C-15 s (35 cycles), and 72 °C-10 min. The products were separated by electrophoresis on a 2% agarose gel from an amplified reaction volume of 20 µL using SYBR® Green Master Mix (Bio-Rad, USA). The icycler iQ real-time detection system analyzed the data, and fold changes were determined using the Ct value. Primers and Their Sequences Used in the Real-Time PCR have been represented in Table S1.

2.10. 2D fluorescent scanning microscopy

2D fluorescent scanning microscopy (Model Leica TCS SP5 STED-CW, Olympus, Germany) was carried out to visualize the permeability variation, niosome uptake by the cells, apoptosis, and cell degradation.

2.11. Hemocompatibility test

Blood samples were drawn into tubes containing 3.8% trisodium citrate anticoagulant in a ratio of 9:1 (v/v). Test and control materials were sterilized by autoclaving and were placed in contact with the anticoagulated whole blood samples. The samples were incubated at 37 °C for 1 h under gentle shaking conditions. After the incubation period, the samples were centrifuged at 3000 rpm for 10 min to separate the red blood cells (RBCs) from the plasma. Next, varying concentrations (1500, 1250, 1000, 750 and 500 µg.mL-1) of SUNI@Nio/Col in PBS (0.8 mL) were mixed with the RBC suspension (0.2 mL) and left undisturbed for 12 h at room temperature. A negative control consisting of PBS was also included. After 12 h, the percentage of hemolysis was determined by measuring the absorbance of the supernatant at 540 nm using a UV–visible spectrophotometer. The percentage of hemolysis was calculated using Eq. (2). Data were analyzed using appropriate statistical methods, and results were expressed as mean ± standard deviation (SD).

$$Percent\ Hemolysis(\%) : (sample\ absorbance - negative\ control\ absorbance / positive\ control\ absorbance - negative\ control\ absorbance) \times 10 \quad (2)$$

2.12. In vivo study

2.12.1. In vivo study protocols and standards

In the current study, the *in vivo* experiments were performed strictly according to the protocols of the National Committee for Ethics in Biomedical Research. 20 female BALB/c inbred mice (weighing 18 ± 2 g, 6–8 weeks) were randomly divided into four groups (5 mice/group). Mice were kept under constant temperature (23 ± 2C), 55% humidity, and 12-h light–dark cycles.

2.12.2. Breast cancer induction and treatment

4 T1 cell line was used to induce breast cancer in mice. Briefly, after counting the cells, 2 million cells were suspended in sterile PBS 1X and then injected subcutaneously into the mice's flank. The measurement of tumor volume was performed with a digital caliper. When an initial

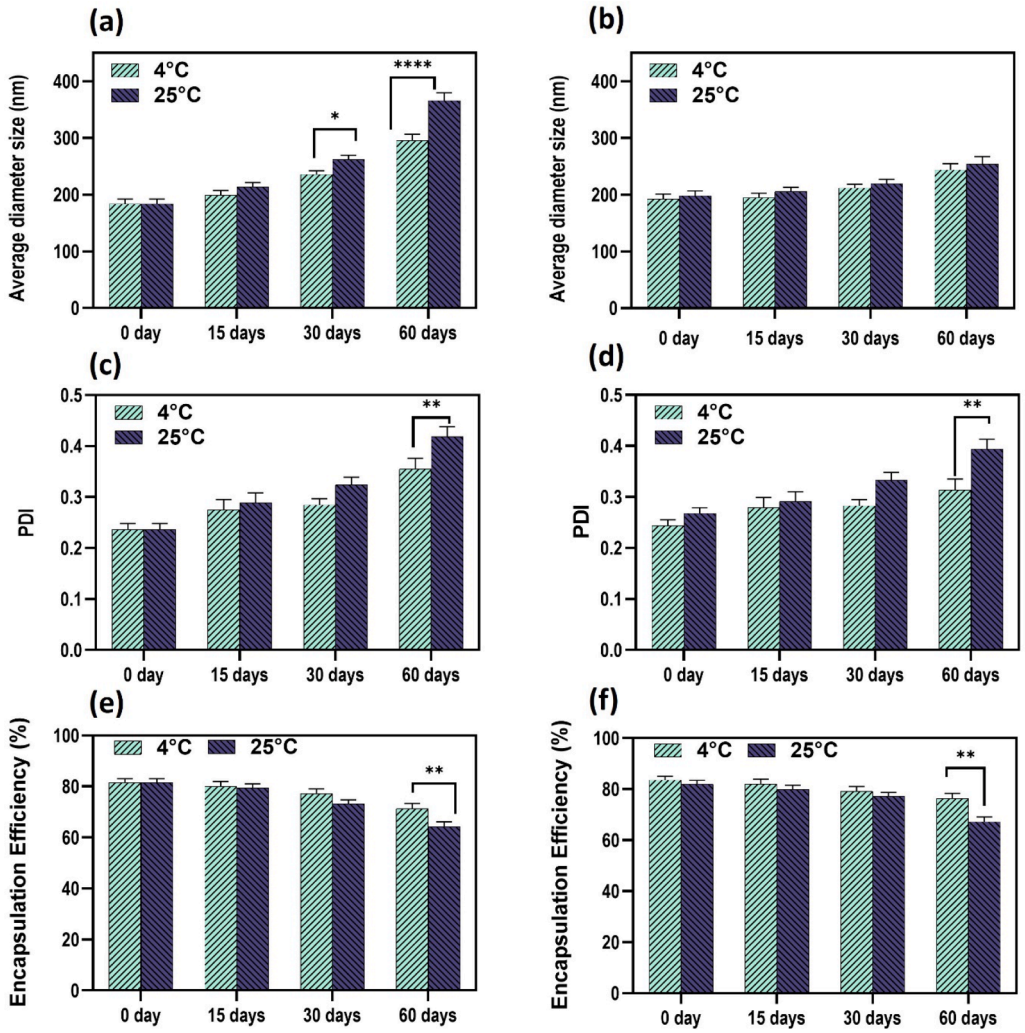

Fig. 5. Size stability evaluation of (a) SUNI@Nio and (b) SUNI@Nio/Col formulations, PDI stability evaluation of (c) SUNI@Nio and (d) SUNI@Nio/Col formulations, EE (%) stability evaluation (e) SUNI@Nio and (f) SUNI@Nio/Col formulations. Data are the average of at least 3 measurements, ***P < 0.001, **P < 0.01, *P < 0.05.

tumor volume of 80 mm^3 appeared, the treatment was started using SUNI@Nio and SUNI@Nio/Col formulations. The intravenous tail injection method was used to deliver the drug formulations on days 1, 5 and 10. After 15 days, the mice were sacrificed; then, the tumors were immediately excised and fixed in a 10% formalin buffer. Mice's body weight was measured every three days during the treatment. The tumor volume measurements were firstly done at the beginning of treatment. After 15 days, the tumors were collected and their size were measured at the end. The calculation of tumor volume was done by the below equation (Eq. (3)).

$$Volume = 1/2 \times \left(width^2\right) \times length \quad (3)$$

2.12.3. In vivo study design

To investigate the efficacy of SUNI@Nio and SUNI@Nio/Col *in vivo*, we used a murine tumor model. Female BALB/c mice were subcutaneously injected with cancer cells to initiate tumor growth. Once the tumors reached a size of approximately 80 mm^3, the mice were randomly divided into three experimental groups with 5 mice in each group:

Group.1 - Cancer control. Group.2 - Mice treated with SUNI@Nio at the dose of 10 mg/kg. Group.3 - Mice treated with SUNI@Nio/Col at the dose of 10 mg/kg. The treatments were administered to the mice via intravenous injection every two days for a total of 14 days. Tumor growth was monitored by measuring tumor volume and body weight of the mice throughout the treatment period. At the end of the study, the mice were sacrificed, and the tumors were excised for further analysis.

3. Results

3.1. Sunitinib-Loaded niosome formulations

The effect of varying the molar ratio of lipid to the drug, surfactant to cholesterol, as well as drug content (as variables) on the physicochemical properties of the niosomes was studied as listed in Table 1. Size, EE, and release were measured as responses to changes in the variables. Based on our previous work (Honarvari et al., 2022), Span 60 with either 10:1 or 20:1 lipid to drug molar ratio exhibited the most desirable properties. In contrast to formulations made using a surfactant-to-cholesterol molar ratio of 1:1, Span 60 formulations prepared using a lipid to drug molar ratio of 10 were smaller and had greater EE. For this reason, a lipid-to-drug molar ratio of 30 was used for the optimized formulations.

According to the present study, the drug content (A), the molar ratio of cholesterol: surfactant(B), and lipid: drug (C) and their respective subfeedbacks regarding size, entrapment efficiency (EE%), and release profile were investigated for optimization (Fig. 1). Table 1 shows the results of the Box-Behnken trials. The size of niosome varied in the range of 191 to 409 nm. As seen, SUNI@Nio has an EE% ranging between

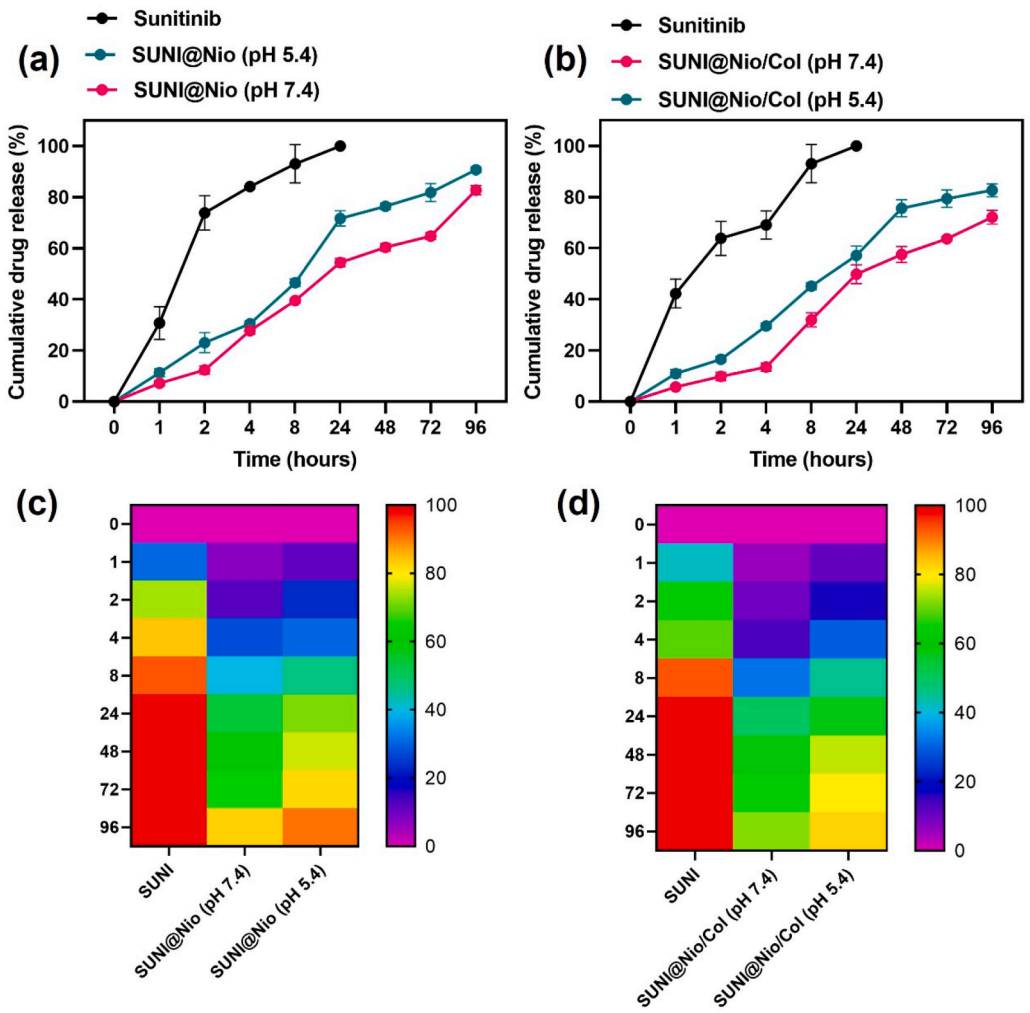

Fig. 6. Comparison of the *in vitro* drug release profiles of (a) free sunitinib, and SUNI@Nio and (b) SUNI@Nio/Col, heat map of (c) SUNI@Nio and (d) SUNI@Nio/Col. Each experiment replicated three. The data is shown as a mean standard deviation.

81.78% and 99.02% (the calibration plot of SUNI represented at Figure S1). Thus, it could be assumed that EE% can be improved by increasing the amount of drug and the ratios of surfactant: lipid and lipid: drug. As shown in Table 1, The release was varied in the range of 42.46 to 67.90 %. In Fig. 2, the % release of niosome formulations is plotted as a response surface. High drug concentrations and high molar ratios between surfactant and cholesterol and lipid to drug boost the release of drugs. Table 1 shows the variance analysis for particle size. Due to its significant p-values, the response was defined as a quadratic model. As a result, drug content strongly influenced the size, surfactant: cholesterol molar ratio, and lipid: drug molar ratio. According to Table 1 independent variables A and C and their relationship to particle size are explained in the regression equation for particle size. However, the particle size was negatively affected by variable B (Fig. 2). The EE% was statistically analyzed and independent factors A and C substantially impacted the EE%. In addition to the F-value, the quadratic pattern has also demonstrated a remarkable correlation. A, B, and C are independent variables that have cumulative effects on EE%, as seen in Table 1. As shown in Fig. 2, independent factors A and C significantly influenced % release. The quadratic model was consequential in terms of its F-value. According to Table 1, A, B, and C have incremental impacts on EE% as disseminated in the regression equation for %release.

As a result, sunitinib-loaded niosomal formulations were formed from the optimized sample coated with collagen. The size of this particle was measured to be 78 nm. As a result of the coating, the size was enhanced.

3.2. Characterization of niosomes

3.2.1. FTIR analysis

Fig. 2 shows FTIR spectra of different ingredients used for niosome preparation as well as those of final formulations. The FTIR spectrum of span 60 exhibited its characteristic absorption bands at 3431 cm^{-1}, (O–H stretching), 1172 cm^{-1} (C-O stretching), 2928 cm^{-1} (C–H stretching), 1730 cm^{-1} (C-O stretching) and 1460 cm^{-1} (C–C stretching). Cholesterol displayed the bands at 2931 cm^{-1} (acetyl group), 2866 cm^{-1} (symmetric CH_3), 1770 cm^{-1} (vinyl group), and 1055 cm^{-1} (C-O group) (Khan et al., 2019). Collagen spectrum showed several characteristic peaks at 3326 cm^{-1} (N–H stretching), 1231 cm^{-1} (C–N group, vibration), 2860–2890 cm^{-1} (C–H group, alkyl), 1669 cm^{-1} (–NH-C = O group) and 1190 cm^{-1} (N–H absorptions of amide III group). In particular, the niosomal formulation exhibits peaks associated with C-O stretching (1172 cm^{-1}), C = O stretching (1746 cm^{-1}), C–H stretching (2800–3000 cm^{-1}), C–H symmetric stretching (1469 cm^{-1}), aliphatic C-N stretching (1000–1250 cm^{-1}), and O–H stretching (3452 cm^{-1}). For collagen-coated niosome, the emerging collagen peaks at the final structure of this formulation indicate successful coating of collagen. As shown in Fig. 3, SUNI@Nio/Col showed similar peaks with peak and intensity reduction with respect to SUNI@Nio/Col indicating sunitinib is encapsulated in SUNI@Nio/Col. The peaks at 2860–2890 cm^{-1} (C–H group, alkyl), and 1669 cm^{-1} (–NH-C = O group) is due to the loading of sunitinib into the final formulation.

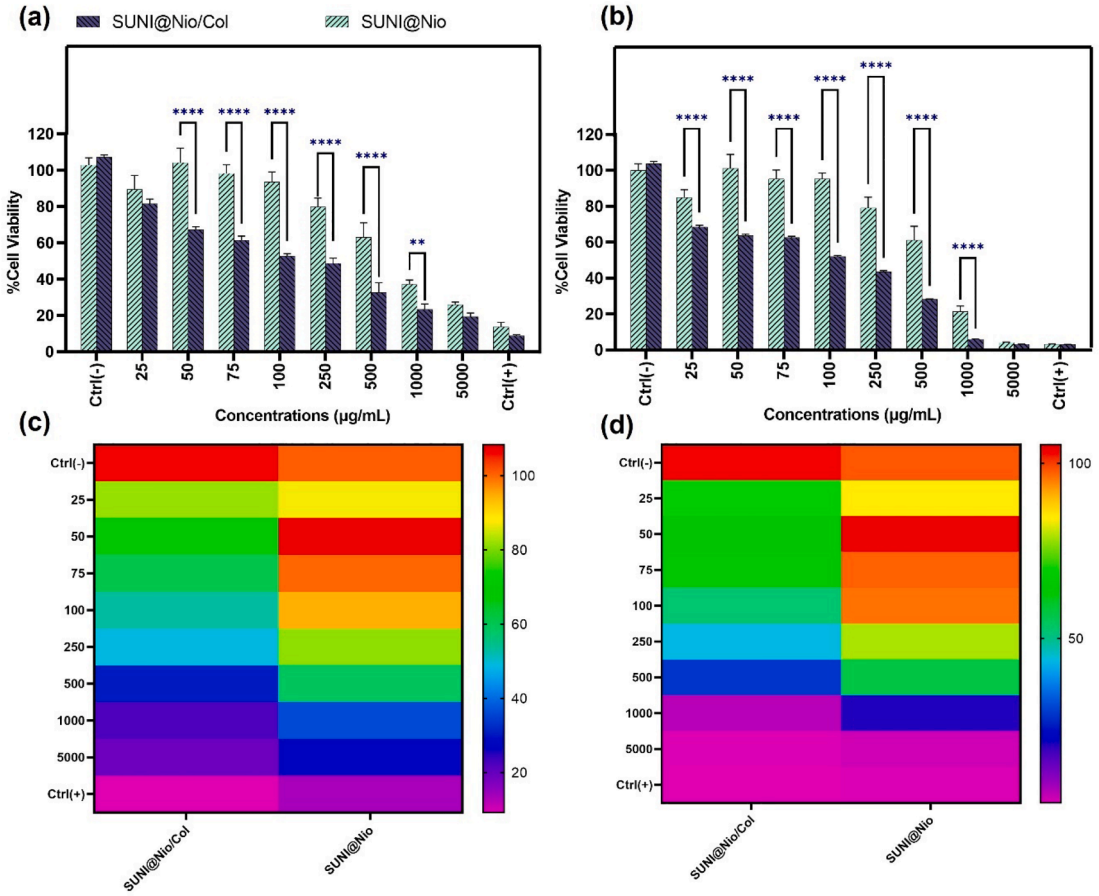

Fig. 7. (a) The effect of SUNI@Nio and SUNI@Nio/Col formulations after 24 h, (b) after 48 h, (c) haet map of SUNI@Nio and SUNI@Nio/Col after 24 h and (d) after 48 h on the viability of A549 cells. Data are represented as mean ± SD and n = 3; ***P < 0.001, **P < 0.01, *P < 0.05.

Table 2
The release kinetic models and the parameters obtained for optimum niosomal formulations containing sunitinib.

Formulations	Zero-order	First-order	Higuchi	Korsmeyer-Peppas	
	R^2 R^2 R^2			R^2	n
SUNI@Nio (pH: 7.4)	0.8253	0.9154	0.9241	0.913	0.4807
SUNI@Nio (pH: 5.4)	0.8026	0.9541	0.928	0.9463	0.441
SUNI@Nio/Col (pH: 7.4)	0.8376	0.9262	0.9241	0.9555	0.5517
SUNI@Nio/Col (pH: 5.4)	0.7691	0.9098	0.928	0.94	0.4347

3.2.1.1. The morphological study. The morphological properties of SUNI@Nio and SUNI@Nio/Col were assessed using TEM and FESEM. Fig. 3a-b shows FESEM micrographs of the SUNI@Nio and SUNI@Nio/Col samples, which have a uniform globular structure characterized by a smooth surface, exhibiting a mean longitude of<100 nm with no bulk components. According to the histogram calculated by ImageJ software, SUNI@Nio has a diameter of approximately 52.25 nm. Compared to SUNI@Nio, there is a slight increase in particle size for SUNI@Nio/Col, with an average particle size of about 71.34 nm. The presence of collagen on the surface of SUNI@Nio/Col and the creation of a large hydrophilic corona can result in such a size increment. TEM assessment was conducted on the inner surface of SUNI@Nio and SUNI@Nio, as shown in Fig. 4c-d. This image shows that the SUNI@Nio and SUNI@-Nio/Col have a spherical shape with a successful collagen coating. Fig. 4 shows the AFM image of SUNI@Nio and SUNI@Nio/Col formulations. As seen, the vesicles exhibited spherical shapes and considerable size variations due to niosome fusion, which may be due to the interactions between mica substrates and niosomes.

3.3. Stability study

Niosomes were tested for their physical stability by comparing their size and the amount of drug maintained in the niosomes before and after two months of storage at two different temperatures. According to previous studies, niosomes are susceptible to swelling as water molecules could penetrate the structure of the niosome, causing them to swell and disintegrate during storage (Mehrarya et al., 2022; Moghtaderi et al., 2022; Rezaei et al., 2022). A calibration curve for the SUNI@Nio/Col was used to determine average size, PDI, and EE at different time intervals and temperatures. As shown in Fig. 5a-d, the size of the SUNI@Nio increased over the storage period. This size increase was especially significant after 1 month at 25 ℃, indicating the lack of suitable stability. However, as for the SUNI@Nio/Col, the size remained nearly constant even after 60 days of storage regardless of the storage temperature. It should be noted, however, that PDI was increased over storage time for both SUNI@Nio and SUNI@Nio/Col.

Regarding EE, temperature and storage time did not significantly affect encapsulation efficiency. Overall, these results showed that the prepared niosomal formulations can be safely stored for up to one month without a significant loss in loaded drug and colloidal stability (Fig. 5e-f).

3.4. The release profile

This research aimed to evaluate how the niosomes structure affected the vesicle's drug release. The original study success in achieving this

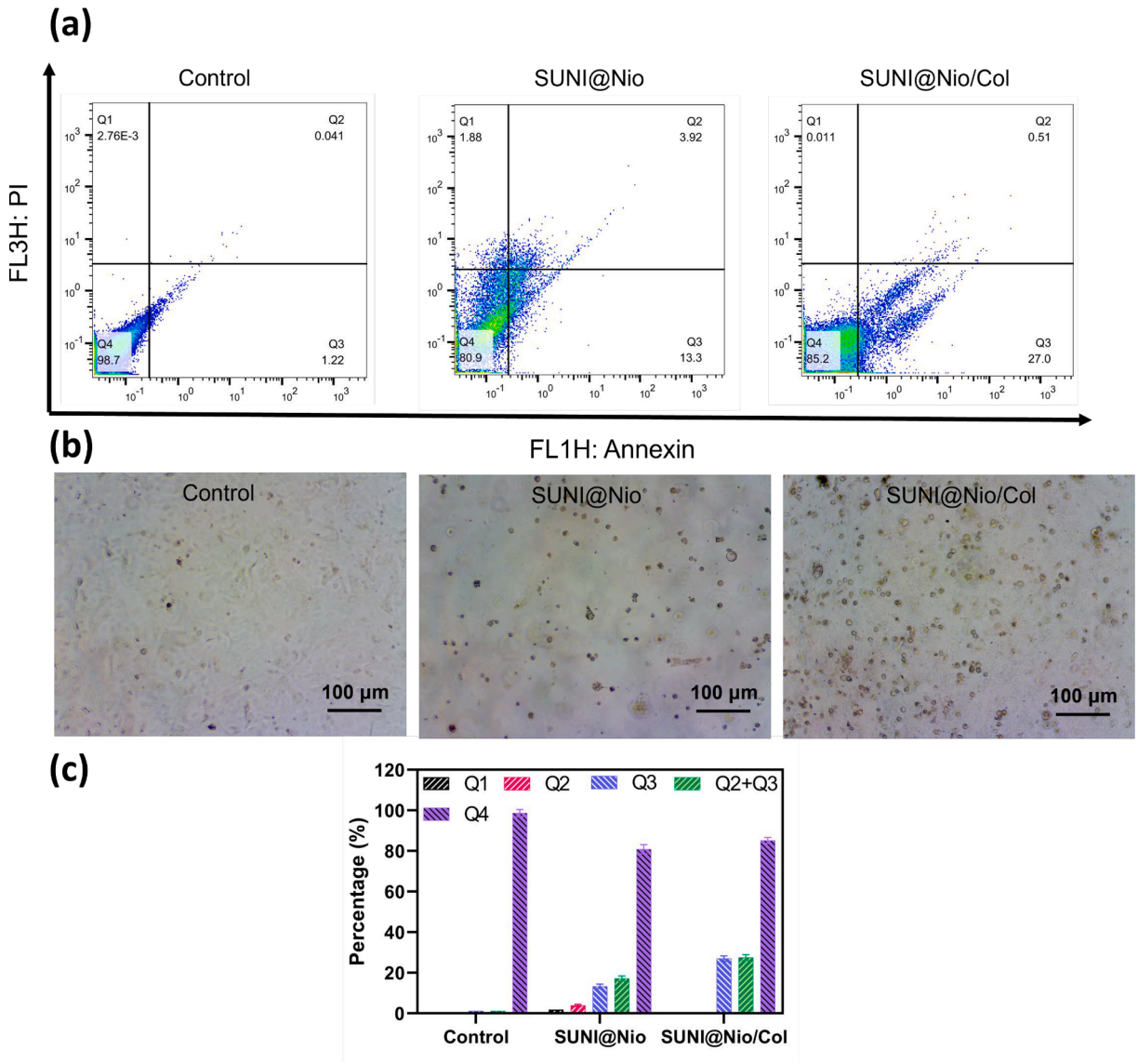

Fig. 8. Flowcytometry analysis of apoptosis in cells treated with SUNI@Nio and SUNI@Nio/Col. (a) Two-dimensional dot plots show the distribution of apoptotic cells (annexin V+/7-AAD +) after treatment with (SUNI@Nio and SUNI@Nio/Col. (b) Cellular images demonstrate the increased rate of apoptosis in cells treated with SUNI@Nio and SUNI@Nio/Col compared to untreated cells. (c) Statistical analysis graph displays the percentage of apoptotic cells in treated and untreated groups. The bars represent the mean ± standard deviation of (each experiments triplicated). Data are represented as mean ± SD and n = 3.

ideal drug release mechanism was a secondary goal attained through the application of kinetic release models. The release profile of sunitinib from the niosome was studied at various pH ranges for about 72 h. Compared to the free sunitinib, the niosomes minimized the initial burst release, with the latter releasing approximately 47–55% of the loaded drug after 24 h, whereas the former released as much as 98% only after 8 h (Fig. 6). The term "release" may seem meaningless for free sunitinib as it is not encapsulated, entrapped or loaded by any carrier and the only restriction for it to be transported into the release media is its limited water solubility. Nevertheless, as a control group, it could provide useful information for comparison with other formulation to elucidate the roles of niosome as well as collagen coating on a sustained release. As seen for SUNI@Nio/Col, a 75% and 77% release rate were released after 48 h at pH 5.4 and 55% and 59% after 48 h at pH 7.4, respectively. At pH values of 7.4 and 5.4, the SUNI@Nio and SUNI@Nio/Col released 65%, 63%, and 84, 78%. of the drug over 72 h, respectively. A decrease in pH resulted in a considerable release of both drugs, as seen in Fig. 7a and b. Niosomes often swell and disintegrate under acidic conditions, which could be due to accelerated hydrolysis of surfactant at acidic pH conditions (Kishore et al., 2011).

Several kinetic models were considered to determine the release kinetics and mechanism of the Sunitinib molecules from the niosome structure at different pH values. It has been indicated that the Korsmeyer–Peppas model ((Mt/M∞) = log Kkp + nlog) fits well for niosome drug release, where n represents the method by which the drug is released. Table 2 presents the parameters of the model and the coefficient (R^2) for all pH values studied. The release data were in accordance with the Korsmeyer-Peppas kinetic model, with n = 0.4401 for SUNI@Nio at pH = 5.4 (which indicates a Fickian diffusion mechanism). For SUNI@Nio/Col at pH = 7.4, n was larger than 0.45, indicating the anomalous diffusion mechanism. Therefore, the Korsmeyer-Peppas kinetic model was the most appropriate to analyze the release data for both formulations (Table 2).

3.5. MTT assay

The MTT test was carried out to test the cytotoxicity of SUNI@Nio as well as SUNI@Nio/Col. The results indicated that SUNI@Nio and

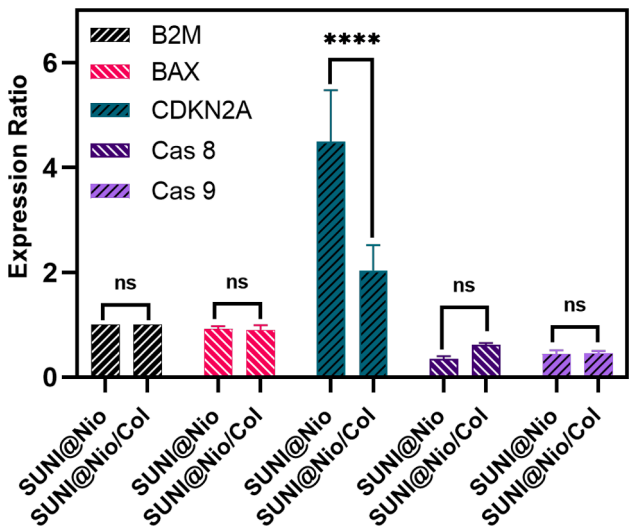

Fig. 9. RT-PCR analysis of gene expression in A549 cells treated with SUNI@Nio and SUNI@Nio/Col. B2M gene was used as a reference (control) and all genes were calculated as relative expression to this control. The graph shows the expression levels of *Bax, CDKN2A, Cas8, Cas9* after treatment with SUNI@Nio and SUNI@Nio/Col compared to untreated cells. The bars represent the mean ± standard deviation of (each experiments triplicated). Data are represented as mean ± SD and n = 3; ****P < 0.0001, ***P < 0.001, **P < 0.01, *P < 0.05.

SUNI@Nio/Col have a great cytotoxicity against the A549 cells (Fig. 7). Compared to free sunitinib, sunitinib-containing niosomes displayed enhanced cytotoxicity against cancer A549 cells. There was a dose-dependent antiproliferative effect in SUNI@Nio/Col. According to several studies, drug-loaded carriers have a more significant cytotoxicity than free drugs at equivalent concentrations (Asadi et al., 2022; Eshrati Yeganeh et al., 2022; Farasati Far et al., 2021; Foroutan et al., 2022). This is due to the fact that a free drug may be able to diffuse freely within a cell. By encapsulating sunitinib molecules in niosomal formulations, sunitinib molecules can be more effectively delivered to cancer cells. Cancer cells have an acidic pH, which increases the drug release rate, thereby resulting in fewer cells survival. The enhanced cytotoxicity of niosomal formulations indicated their great potential for drug delivery.

3.6. Flow cytometry

Flow cytometry can detect apoptosis in its early stages by conjugating annexin V with fluorescein isothiocyanate (FITC). The penetration of the cellular membrane changes during other apoptosis steps, and some staining colors become permeable to the cells, while the same colors are not permeable to live cells. Staining DNA with PI during the last steps of the apoptosis process makes it possible to distinguish between live and dead cells. Apoptosis steps can be classified using different staining colors to distinguish between apoptotic, necrotic, dead, and living cells. Different niosomal formulations were used in IC_{50} concentrations for 24 h to measure different apoptosis steps in A549 cells, followed by flow cytometry using FITC and PI staining. Based on Fig. 8, the control group (Q4 region) has a higher percentage of living cells (96%) than other groups. The total apoptosis death is calculated from Q2 + Q3. According to the results, the drug caused much more apoptotic death in treated cells than it did in the untreated cells as a control group. Furthermore, the total apoptosis induced by SUNI@Nio/Col was 28% which is significantly higher than that in SUNI@Nio, I.e., 16%, further supporting the cytotoxicity results obtained above.

3.7. Apoptotic gene expression analysis (RT-PCR)

All the formulations have inhibitory properties, influencing the expression levels of several genes within the lung cancer cells. Real-time polymerase chain reaction analysis was used to determine the transcriptional levels of apoptotic *B2M*, *Bax*, *CDKN2A*, *Cas8*, and *Cas9* genes in treated malignant cells (Fig. 9). The expression levels of *CDKN2A* and *Bax* were significantly higher in A549 cancer cell lines exposed to SUNI@Nio and SUNI@Nio/Col for 24 h compared to the control group, whereas the expression levels of *Cas8, Cas9*, and *Bax* were significantly lower (Fig. 9). Also, Table S2 represent the SUNI@Nio and SUNI@Nio/Col gene expression data.

3.8. Scratch assay

As tumor cell migration is one of the conditions for cancer metastasis, the effect of SUNI@Nio and SUNI@Nio/Col niosomal formulation on the motility of A549 cells was examined using a wound scratch experiment. Using SUNI@Nio and SUNI@Nio/Col, the percentage of the total area covered in the treated cells appeared to drop significantly when compared to the blank group (non-transfected A549 cells; Fig. 10). In addition, SUNI@Nio/Col showed more migration suppression compared to SUNI@Nio, which demonstrated potent *in vitro* migration. In addition, the results showed that the empty niosome did not differ significantly from the control in tests conducted just on cells (control).

3.9. ELISA test (Cas-3 and Cas-7 protein degradation-final apoptotic pathway)

Caspases are a group of protease enzymes that play an important and key role in the occurrence of inflammatory responses, differentiation, and programmed cell death. These enzymes play an essential role in initiating the cascade process of apoptosis and inducing it to cells. Their dysfunction can cause diseases such as cancer. As a result, in cancer treatment methods, one of the methods is the induction of apoptosis through caspases cascade activity. Apoptosis, a form of programmed cell death linked to the action of the caspase enzyme, plays a crucial role in maintaining homeostasis in multicellular animals. This means that direct imaging of apoptosis in living cells has the potential to improve significantly disease diagnosis, drug development, and therapy monitoring. Direct apoptosis imaging, however, has not been fully verified, particularly for live cells in *in vitro* and *in vivo* settings. In this study, we tested the viability of a technique allowing us to see active *Cas3* and *Cas7* in real time inside living cells. Furthermore, the cysteine-aspartic acid proteases *Cas3* and *Cas7* can immediately execute apoptosis, and subsequent execution of apoptosis requires sequential activation from *Cas8* or *Cas9* activation (Fig. 11). For this reason, Asp-Gly-Val-Asp (DEVD), a peptide substrate for *Cas3* and *Cas7*, has been widely used as a caspase-cleavable imaging probe for apoptosis imaging and the tracking of caspase activity in tumor cells under *in vitro* settings (Shim et al., 2017). Figure S2 represent the control standard calibration of *Cas3/Cas7* and the activity of SUNI@Nio and SUNI@Nio/Col.

3.10. 2D fluorescent microscopy

2D fluorescent microscopy was used to examine how effectively the niosomes penetrated and internalized into cancer cells. Using this technology, researchers have also measured how well cancer cells uptake niosomes (Honarvari et al., 2022). Since sunitinib has fluorescent activity, there was no need to label the target cells before imaging. Fig. 12 shows how two distinct color panels can be combined through careful color mixing to reveal the co-localization of the drug and the labeled cell and its subsequent internalization. The depth of the resulting shade accurately reflects the degree to which the individual components of the mixture are overlapping and co-localizing.

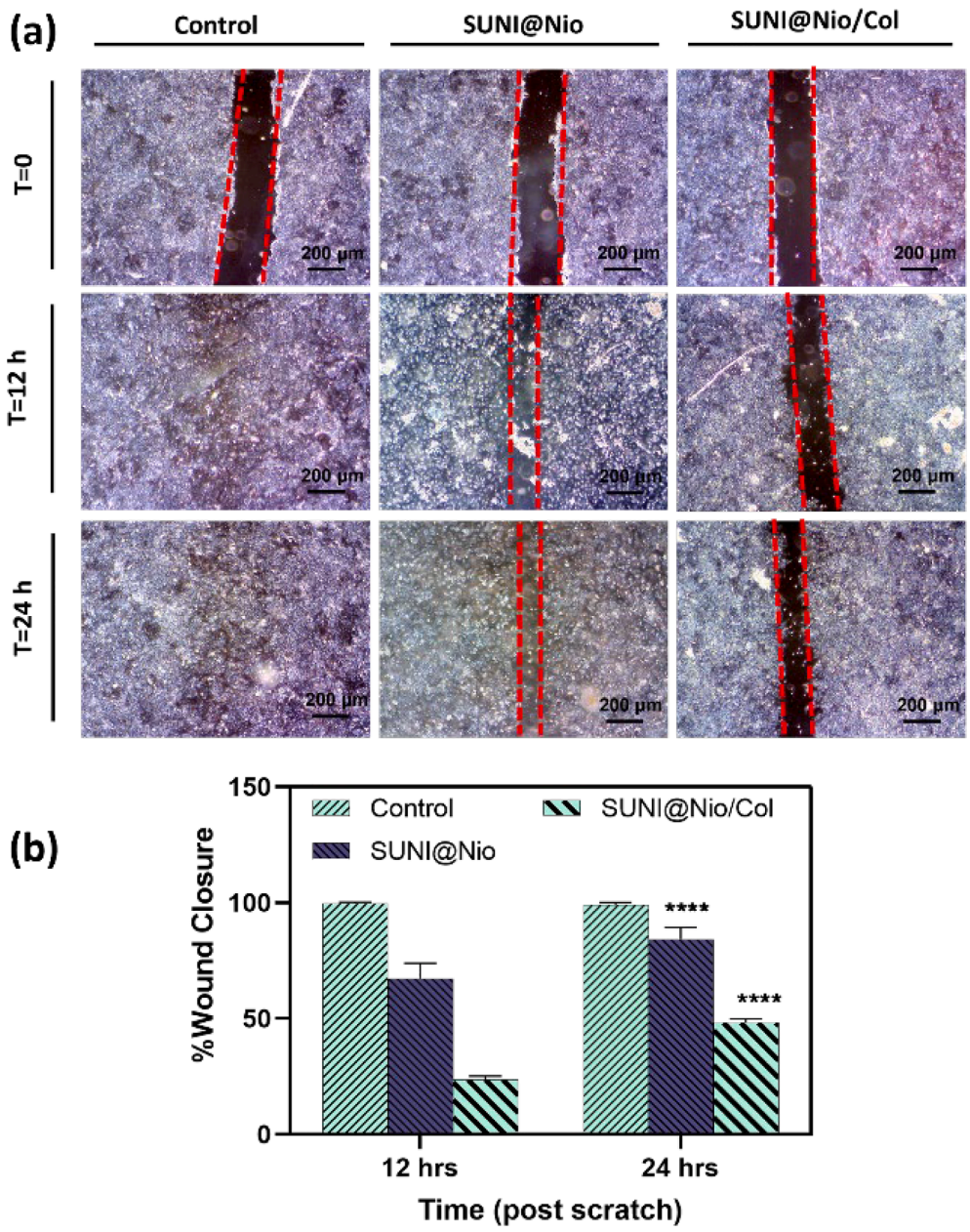

Fig. 10. In vitro Scratch Wound Healing Analysis of A549 Cells. (a) Time-course images demonstrating the rate of scratch wound closure in A549 cells with control (t = 0, t = 12 h, and t = 24 h), SUNI@Nio, and SUNI@Nio/Col treatments. (b) Quantitative representation of wound closure percentage at the indicated time points in the scratch wound assay, demonstrating a significant inhibition of cell migration in the presence of SUNI@Nio and SUNI@Nio/Col compared to the control.

3.11. Hemocompatbaility test

Proper evaluation of the biocompatibility of materials intended for use in the biomedical field is essential. One reliable and scientific method for determining a synthetic material's biocompatibility with living systems is the hemolytic activity test (Yeganeh et al., 2022b). Although most nanoparticles encounter blood at some point during their path through the body, nanoparticle hemocompatibility is often overlooked. These particles can affect the morphology of red blood cells (RBCs), causing hemolysis when the cell membrane is ruptured, and the cells are lysed. These negative interactions between nanoparticles and the bloodstream can lead to increased inflammatory and autoimmune diseases, infection, and malignancy by inciting the immune system to suppress (Gong et al., 2020). In this study, the blood compatibility of SUNI@Nio/Col was examined (Fig. 13). Hemolysis percentages lower than 5% were obtained for for all concentrations of SUNI@Nio/Col (1500, 1250, 1000, 750, and 500 µg.mL^{-1}) which is considered to be safe (Li et al., 2016). Hemolysis percentages lower than 5% are considered safe for all concentrations of SUNI@Nio/Col (1500, 1250, 1000, 750, and 500 µg.mL-1). The nanoformulation demonstrated a safe system for hemolysis of human erythrocytes, possibly due to the inclusion of Col, which facilitates NP escape from the reticuloendothelial system and prevents macrophage scavenging.

3.12. Mice body weight and tumor volume

After the treatment period, the changes in mice's weights and tumor volumes were assessed. According to the results (Fig. 8E), the body weight of mice treated with SUNI@Nio and SUNI@Nio/Col demonstrated a statistically significant increase in comparison with the control. However, no significant body weight changes were observed in SUNI@Nio and SUNI@Nio/Col in comparison with each other. The

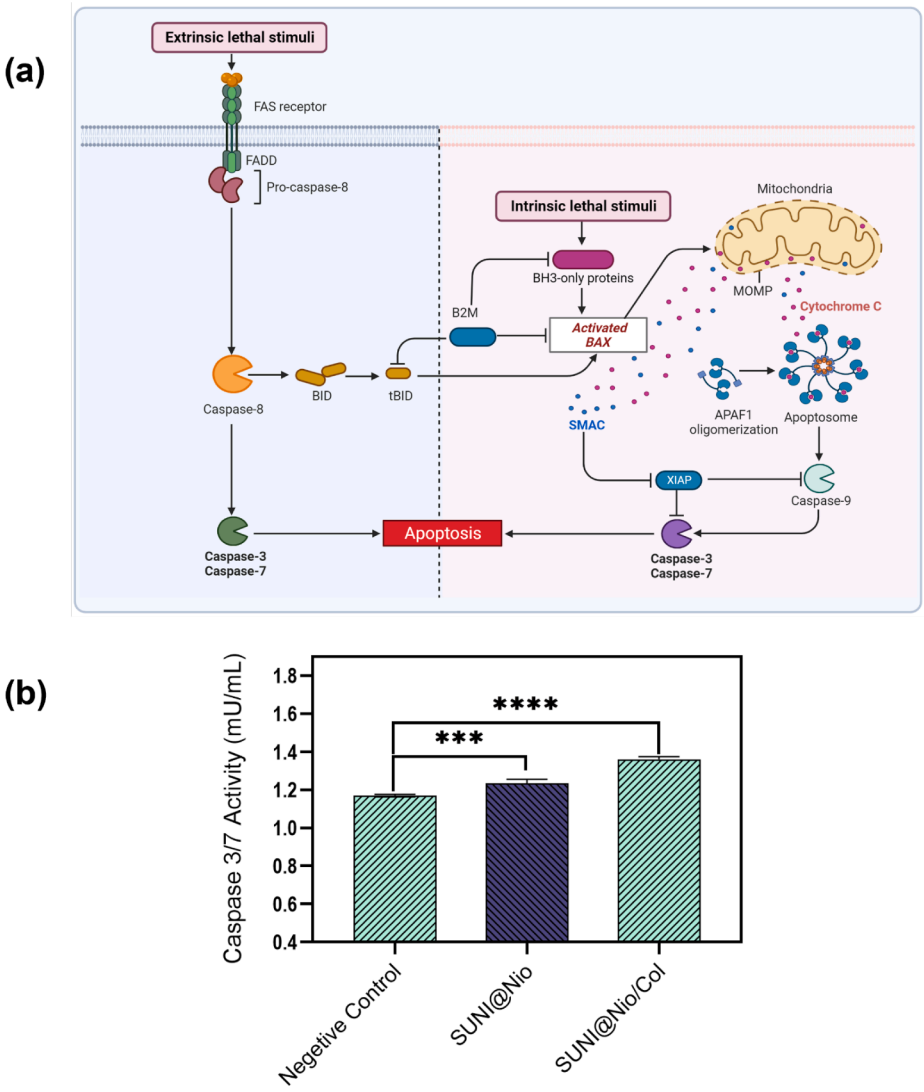

Fig. 11. ELISA analysis of *Cas3* and *Cas7* expression in apoptosis pathways. (a) Depiction of the intrinsic and extrinsic pathways leading to apoptosis through activation of *Cas3* and *Cas7*. (b) the statistical expression of *Cas3* and *Cas7*, demonstrating the differential involvement of these two caspases in apoptotic processes. The bars represent the mean ± standard deviation of (number of experiments or replicates was 3). Data are represented as mean ± SD and n = 3; ****P < 0.0001, ***P < 0.001, **P < 0.01, *P < 0.05.

changes in breast tumor volume between the control group and either SUNI@Nio and SUNI@Nio/Col, were considerable, and a significant reduction was observed. In the comparison of SUNI@Nio and SUNI@-Nio/Col, a significant decrease was observed (Fig. 14).

4. Discussion

This research aims to create a niosomal formulation of sunitinib that may be used to specifically target and treat lung cancer. Table 1 displays the range of niosomal formulations, each with its unique lipid-to-drug molar ratio, and EE. The EE and particle size of a niosomal formulation are highly dependent upon the utilized surfactants, cholesterol (i.e. lipid), and their ratio, as these factors determine hydrophilic-lipophilic balance (HLB) value which is the most important characteristic in niosome, liposome and emulsion formation. (Mehrarya et al., 2022). The niosomes made up of Span 60 are relatively small due to the enhanced hydrophilic-hydrophobic interaction between the encapsulated sunitinib, cholesterol, and the hydrophobic chain of the surfactant (Sahrayi et al., 2021). Niosomes with a lipid-to-drug ratio of 10 were significantly smaller than those with a ratio of 20. These findings corroborated previous research suggesting that increasing the lipid concentration could increase the niosome size and the thickness of the lipid bilayer (Honarvari et al., 2022). Size is one of the most important factors in how well a drug is entrapped and how quickly it is released. According to previous findings, This study showed that the size distribution is strongly affected by changes in cholesterol levels, where larger vesicles were observed as the cholesterol levels raised (Moghtaderi et al., 2022). As a measure of niosome uniformity, the PDI value can be used to evaluate how stable the system is and how consistent the particle size is (Mobaraki et al., 2022). In a range from 0 to 1, the suspension with a lower PDI value is more uniformly distributed. In addition to a narrow size distribution, the homogeneous particles have a low propensity to agglomerate (Yeganeh et al., 2022a). These results are in agreement with those of previous studies on niosomes (Farmoudeh et al., 2020; Khan et al., 2020). In fact, if the cholesterol concentration is high, changes in the bilayer structure may occur, possibly resulting in decreased drug retention. To achieve the highest loading and colloidal stability, it is important to choose an appropriate cholesterol ratio to optimize EE and size simultaneously. The size measured by FESEM, and TEM were found to be significantly lower than the values obtained by Nano Zetasizer (DLS). The drying procedure carried out in the sample preparation for FESEM, and TEM images could be responsible for this discrepancy, as the particles could shrink. As a result, FESEM and TEM can be used to calculate the average size of niosomes. DLS, on the other hand, measures the hydrodynamic diameter, which incorporates the core as well as any surface-bound or adsorbate molecules (such as ions and water molecules) (Farasati Far et al., 2022c; Sahrayi et al., 2022b; Yeganeh et al., 2022b). In other words, the latter takes the dangling chains or swollen coated layer_ the

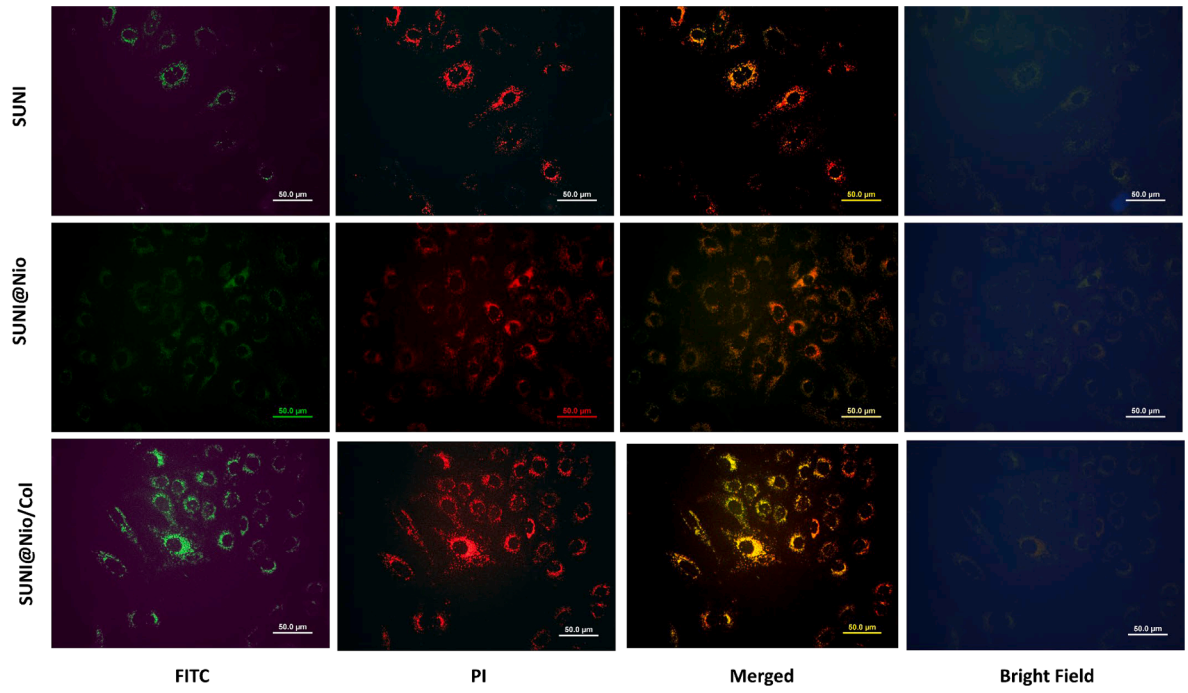

Fig. 12. Intracellular uptake 2D-fluorescence images after 1 h of treatments at 37 °C with 95% humidity. Green panel represent fluorescein isothiocyanate (FITC) channel. FITC is a commonly used fluorescent dye that emits green light when excited by the laser in 2D fluorescent systems. Propidium iodide (PI) is also commonly used fluorescent dyes that emit red light when excited by the laser in a 2D fluorescent systems. They are often used to label and visualize cellular structures, proteins, and other biomolecules in biological samples. The red channel in 2D fluorescent images is typically used to visualize the PI-labeled structures, and the information captured in the red channel is usually combined with other channels, such as green channels, to form a composite color image.

coated collagen in this case_ into account for size measurement as they too scatter the laser/light. Drug release kinetics are affected by bilayer membrane fluidity and lipid composition. Furthermore, electrostatic attraction/repulsion forces between the drug and surfactant are crucial as they may become charged under physiological conditions (Farasati Far et al., 2022a). In the first stage, sunitinib is released at a rapid pace, and in the second stage, it is released at a slower rate (Bhia et al., 2021). The early burst release can be ascribed to the dissociation of drug molecules from the vesicle membrane, which was followed by a slower phase due to slow drug diffusion across the bilayers (Bianchini et al., 2019). Table 2 displays the R^2 values of various release kinetic models, indicating that diffusion and erosion are the primary regulators of drug release (Shaddel et al., 2022). The Higuchi equation models drug diffusion. Drug release from a polymeric nanoparticle dosage form is described and studied using the Korsmeyer-Peppas model because it follows various kinetic modes, including diffusion, Fickian transport, and non-Fickian transport. Key to the zero-order model, which describes a system in which the rate of drug release is independent of drug concentration, is the process of dissolution. First-order rate equations capture concentration dependencies, such as the one that describes how quickly a drug is released. The n value in the range of 0.43 to 0.85 also suggests that the release is based on Fickian diffusion (Asadi et al., 2022). Niosomes may be more stable when stored at 4 °C because the bilayer is less likely to move around (Sahrayi et al., 2022a). Vesicle fusion or aggregation may be linked to growth in size during storage (Foroutan et al., 2022). Further increasing volume of lipid vesicles and drug leakage at elevated temperatures may contribute to the decline in EE % (Liu et al., 2019). Additionally, at elevated temperatures, the fatty acid chain in the surfactant molecule melts, resulting in a decrease in the vesicle thickness and higher chain mobility which is associated with a greater diffusion rate (Shahgholi et al., 2022a). In addition, due to the disorganized fatty acid chain of the surfactants, bilayer thickness decreases, and the diffusion rate increases when temperatures rise. (Shahgholi et al., 2022b). Sunitinib tablets 37.5 mg qDay (GIST and RCC) have been approved by the US FDA for use in the initial treatment of advanced or metastatic lung cancer (Blumenschein et al., 2012). Moreover, a higher cytotoxic effect against cancer cells has been observed when this drug has been formulated with niosome, requiring one to use lower amount of drug, which is accompanied by less side effect on healthy organs/tissues. The dose–response relationship between sunitinib and toxicity was observed in studies where cancer cells were treated with either free sunitinib or a niosome loaded with sunitinib. Intriguingly, the data demonstrated that the cytotoxicity effect of free sunitinib was less than that of sunitinib-loaded niosomes at the same dose. These results might make sense if niosomal encapsulation of the drug increased its antiproliferative activity. Niosomes devoid of drugs had no cytotoxic effect on treated cells, as predicted. This result substantiated that niosomes are safe for use as a drug delivery mechanism in humans. Sunitinib and sunitinib-loaded niosomes caused cytotoxicity in A549 cells via inducing apoptosis, as shown by flow cytometric analysis. The drug's mechanism of action was not altered by the process of preparing the niosomes. These findings corroborate previous research showing that the ratio of pro- to anti-apoptotic proteins, such as those encoded by the *Bax* and *CDKN2A* genes, is crucial for the development and expansion of cancer cells (Chen et al., 2021). The amount of RNA encoding *CDKN2A* was upregulated significantly. Increased expression of proteins involved in apoptosis, like *Bax* and *CDKN2A*. Nanoparticles' ability to localize and penetrate cells is an intriguing topic for further research. Hybrid lipid polymer nanoparticles improve the anticancer activity of sunitinib malate in lung cancer by entering cancer cells, diffusing in the cytoplasm, and avoiding breakdown in endosomes (Ahmed et al., 2022). Sunitinib improved drug delivery in pancreatic neuroendocrine tumors was achieved via injectable hydrogels made of CS modified with methacrylate groups (MA) (Keutgen et al., 2021). Studies have shown that oxaliplatin-niosomes and paclitaxel-niosomes are also effective drug delivery methods for treating colorectal cancer. (El-Far et al., 2022). Results from confocal imaging indicated that, while encapsulated sunitinib was mostly localized in the cytoplasm via the

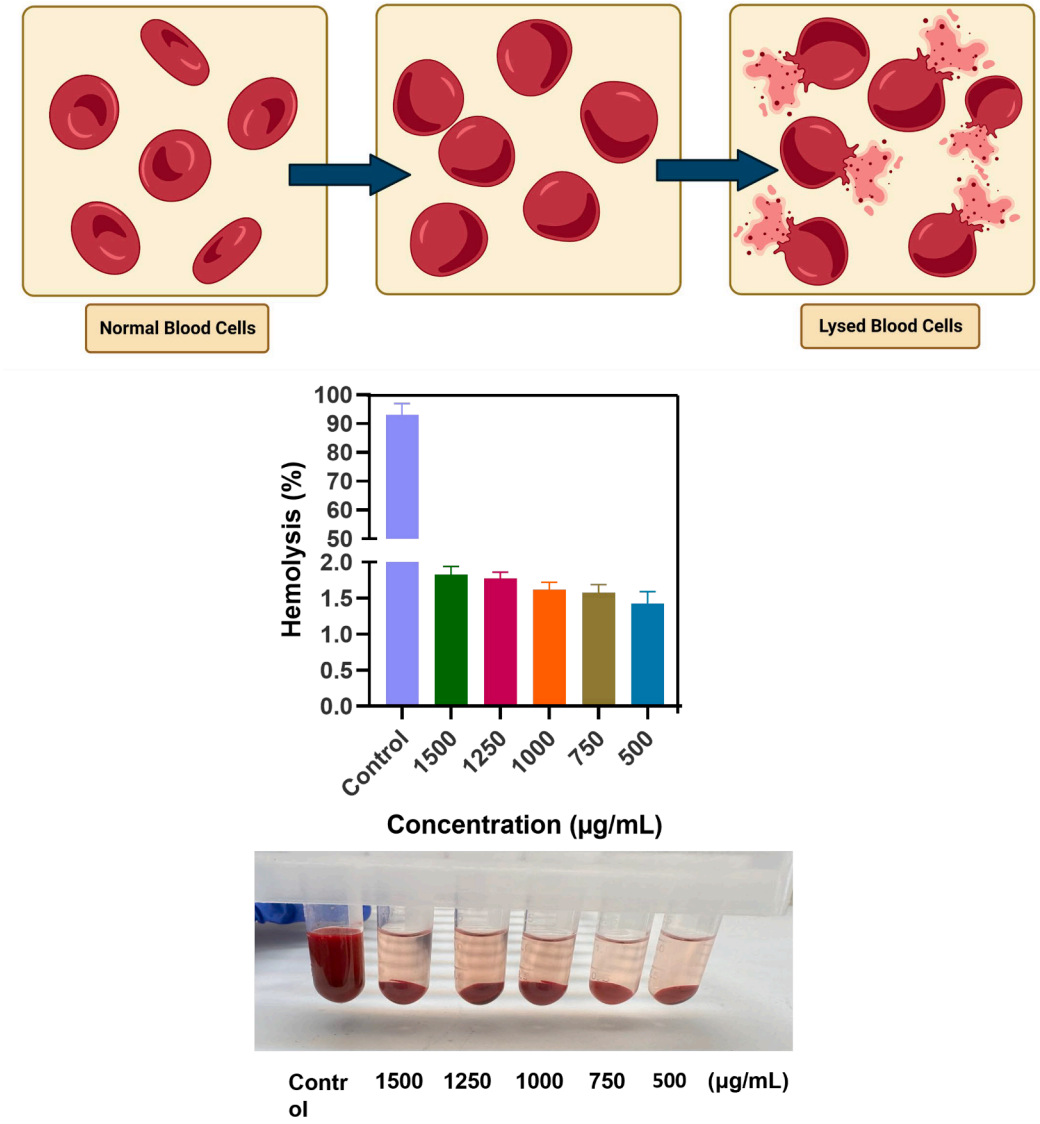

Fig. 13. The hemolysis percentage of SUNI@Nio/Col nanoformulation was evaluated in comparison to a positive control (SDS: sodium dodecyl sulfate) at varying concentrations. Fresh whole blood samples were obtained from healthy human volunteers and were exposed to different concentrations (1500, 1250, 1000, 750 and 500 µg.mL^{-1}) of SUNI@Nio.

endocytosis pathway, free sunitinib accumulated in the membrane of cancer cells and entered slowly via a diffusion-limited transport mechanism (Lim et al., 2015). These studies corroborate our fluorescence microscopy findings, which show that drug-loaded niosomes are more effective at penetrating cancer cells and causing cell death (i.e., toxicity and apoptosis).

In summary, previous studies on sunitinib drug delivery have primarily focused on developing various types of nanocarriers, including liposomes, polymeric nanoparticles, and solid lipid nanoparticles, to enhance the solubility and stability of sunitinib, as well as to improve its pharmacokinetics and efficacy. Many of these studies have reported improved *in vitro* anticancer activity of sunitinib, but there remains a need for a delivery system that provides both enhanced uptake and controlled release of the drug *in vivo*.

Our study differs from previous studies in several keyways (Table 3). First, we used nanoniosomes, a novel type of nanocarrier, to encapsulate sunitinib. Unlike liposomes and polymeric nanoparticles, nanoniosomes are composed of a mixture of phospholipids, cholesterol, and surfactants, which gives them a unique combination of properties that are well-suited for drug delivery. Second, we developed a controlled release mechanism for sunitinib, which allows for more sustained exposure of the drug to cancer cells over an extended period of time. Also, our study demonstrates improved uptake of sunitinib by cancer cells, which is a critical factor in determining the overall efficacy of the drug. Overall, our study provides new insights into the development of sunitinib-loaded nanoniosomes as a promising drug delivery system. Our findings demonstrate the potential of nanoniosomes to provide both improved uptake and controlled release of sunitinib, leading to enhanced *in vitro* anticancer activity compared to previous studies. Finally, the present study investigated the *in vivo* efficacy of SUNI@Nio and SUNI@Nio/Col against breast cancer in a mouse model. The results indicated that the treatment with both SUNI@Nio and SUNI@Nio/Col resulted in a significant reduction in tumor volume compared to the control group, highlighting the potential anti-cancer activity of sunitinib when delivered via niosomes. Moreover, the observed increase in body weight of the treated mice suggests that the formulations were well-tolerated and did not cause any significant toxicity. Interestingly, no significant difference was observed in body weight changes between the SUNI@Nio and SUNI@Nio/Col groups, indicating that the addition of Col did not affect the safety of the formulation.

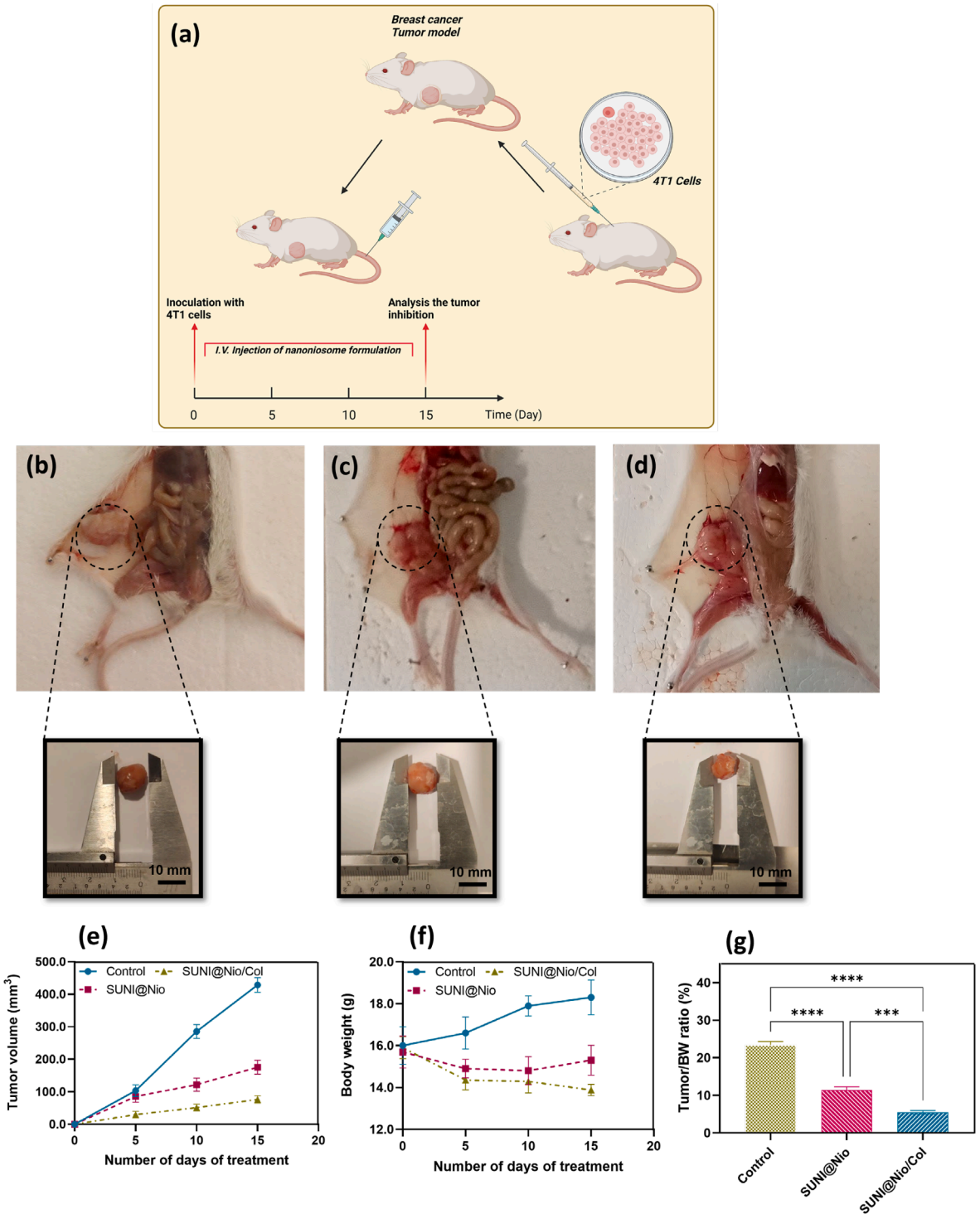

Fig. 14. The results of an *in vivo* therapeutic experiment in 4 T1-tumor bearing nude mice, aimed at investigating the efficacy of different treatments in reducing tumor growth while minimizing adverse effects in terms of body weight. (a) the experimental process, which involved administering various formulations to the mice over the course of 14 days, (b) the control group, which received no treatment, (c) and (d) show two experimental groups that received SUNI@Nio, SUNI@Nio/Col, respectively, (e) the change in tumor volume over time for each group, (f) the corresponding change in body weight. (g) the tumor-to-body weight ratio of untreated mice and mice treated with the different formulations, demonstrating that SUNI@Nio/Col was the most effective treatment in reducing tumor growth while minimizing body weight loss. The results suggest that SUNI@Nio/Col has potential as a targeted and safe therapy for cancer treatment. The sample size for each group was n = 5.

Table 3
An overview of the previous studies of sunitinib drug delivery.

Study	Drug Delivery System	Outcome	Key findings	Disadvantages/Gaps	Ref
Dolman et al. (2012)	Dendrimers	Improved targeting and enhanced therapeutic efficacy	Sunitinib was conjugated to dendrimers, which showed improved targeting to cancer cells and enhanced therapeutic efficacy.	Difficulty in large-scale production	(Dolman et al., 2012)
Maitani et al. (2012)	Pegylated liposomes	Controlled release and improved therapeutic efficacy	The pegylated liposomal system allowed for the controlled release of sunitinib, leading to improved therapeutic efficacy.	Limited stability under high temperature conditions	(Maitani et al., 2012)
Altintas et al. (2013)	Albumin nanoparticles	Improved pharmacokinetics and anti-tumor efficacy	Sunitinib was loaded into albumin nanoparticles, resulting in improved pharmacokinetics and anti-tumor efficacy compared to the free drug.	Potential immunogenicity of the albumin nanoparticles and challenges in maintaining stability during storage	(Altintas et al., 2013)
Joseph et al. (2016)	Chitosan nanoparticles	Improved stability and targeting	Sunitinib was loaded into chitosan nanoparticles, resulting in improved stability and targeted delivery to cancer cells compared to the free drug.	Reduced drug loading capacity	(Joseph et al., 2016)
Tran et al. (2016)	Polymeric nanocapsules	Controlled release and improved pharmacokinetics	Sunitinib was loaded into polymeric nanocapsules, allowing for controlled release and improved pharmacokinetics compared to the free drug.	Challenges in maintaining stability during storage	(Tran et al., 2016)
Scrivano et al. (2017)	Hyaluronic acid conjugates	Improved targeting and reduced toxicity	Sunitinib was conjugated to hyaluronic acid, allowing for improved targeting to cancer cells and reduced toxicity compared to the free drug.	Challenges in maintaining stability during storage and potential immunogenicity of the conjugate	(Scrivano et al., 2017)
Saber et al. (2017)	Gold nanoparticles	Enhanced therapeutic efficacy and targeted delivery	Sunitinib was conjugated to gold nanoparticles, resulting in enhanced therapeutic efficacy and targeted delivery to cancer cells.	Costly and complex synthesis process	(Saber et al., 2017)
Yang et al. (2018)	Near-infrared light-activatedliposomes	Controlled release and improved therapeutic efficacy	The pH-sensitive liposomal system allowed for the controlled release of sunitinib, leading to improved therapeutic efficacy.	Reduced stability at extreme pH conditions	(Yang et al., 2018)
Freitas et al. (2018)	Solid lipid nanoparticles	Improved oral bioavailability	The use of solid lipid nanoparticles resulted in improved oral bioavailability of sunitinib in both *in vitro* and *in vivo* studies.	Limited ability to target specific tissues	(Freitas et al., 2018)
Bianchini et al. (2019)	Polyethylene glycol (PEG)-modified liposomes	Controlled release and improved pharmacokinetics	The PEG-modified liposomal system allowed for the controlled release of sunitinib, leading to improved pharmacokinetics compared to the free drug.	Reduced stability under high temperature conditions	(Bianchini et al., 2019)
Yongvongsoontorn et al. (2019)	Micellar nanocarriers	Improved solubility and stability	Sunitinib was conjugated to micellar nanocarriers, resulting in improved solubility and stability compared to the free drug.	Challenges in controlling drug release rate	(Yongvongsoontorn et al., 2019)
Otroj et al. (2020)	Poly(lactide-co-glycolide) (PLGA) nanospheres	Improved therapeutic efficacy and reduced toxicity	Sunitinib was encapsulated in PLGA nanospheres, leading to improved therapeutic efficacy and reduced toxicity compared to the free drug.	Limited control over release rate	(Otroj et al., 2020)
Han et al. (2020)	Cyclodextrin-based nanoparticles	Improved solubility and stability	Sunitinib was successfully encapsulated in cyclodextrin-based nanoparticles, which resulted in improved solubility and stability compared to the free drug.	Potential for toxicity from the use of cyclodextrins	(Han et al., 2020)
Streets et al. (2020)	Polymeric micelle nanoparticles	Improved stability and controlled release	Sunitinib was loaded into polymeric micelle nanoparticles, resulting in improved stability and controlled release of the drug.	Possible immune response to the nanoparticle components	(Streets et al., 2020)
He et al. (2020)	Lipid-based nanoparticles	Improved therapeutic efficacy and reduced toxicity	Sunitinib was encapsulated in lipid-based nanoparticles, leading to improved therapeutic efficacy and reduced toxicity compared to the free drug.	Limited control over release rate	(He et al., 2020)
Cleland et al. (2020)	Dendrimers	Improved solubility and stability	Sunitinib was conjugated to dendrimers, resulting in improved solubility and stability compared to the free drug.	Difficulty in large-scale production	(Cleland et al., 2020)
Razmimanesh et al. (2021)	Polymeric nanoparticles	Improved solubility and stability of sunitinib	Sunitinib was successfully loaded into polymeric nanoparticles, resulting in enhanced solubility and stability compared to the free drug.	Limited control over release rate	(Razmimanesh et al., 2021)
Jafari et al. (2021)	Hydrogel nanocomposites	Improved pharmacokinetics and reduced toxicity	Sunitinib was loaded into hydrogel nanoparticles, resulting in improved pharmacokinetics and reduced toxicity compared to the free drug.	Challenges in controlling drug release rate	(Jafari et al., 2021)

(*continued on next page*)

Table 3 (*continued*)

Study	Drug Delivery System	Outcome	Key findings	Disadvantages/Gaps	Ref
Zhang et al. (2021)	Metal-organic frameworks	Enhanced solubility and stability	Sunitinib was encapsulated in metal–organic frameworks, resulting in improved solubility and stability compared to the free drug.	Limited drug loading capacity and challenges in maintaining stability during storage	(Zhang et al., 2021)
Ahmed et al. (2022)	Hybrid nanocarriers	Improved targeting and enhanced therapeutic efficacy	A hybrid nanocarrier system was developed for sunitinib, resulting in improved targeting to cancer cells and enhanced therapeutic efficacy compared to the free drug.	Challenges in maintaining stability and specificity during the synthesis process	(Ahmed et al., 2022)
Tavakoli et al. (2022)	Liposomal nanocarriers	Improved targeting and therapeutic efficacy	Sunitinib was encapsulated in liposomal nanocarriers, leading to improved targeting and therapeutic efficacy compared to the free drug.	Challenges in maintaining stability during storage	(Tavakoli et al., 2022)
Torabi et al. (2023)	Mesoporous silica nanoparticles	Controlled release and improved targeting	Sunitinib was loaded into mesoporous silica nanoparticles, allowing for controlled release and improved targeting to cancer cells compared to the free drug.	Challenges in maintaining stability during storage and potential toxicity of the nanoparticle	(Torabi et al., 2023)

5. Conclusions

Niosomal sunitinib was shown to be an effective, safe, and sufficient delivery method in the current investigation. In physiological settings, the synthesized SUNI@Nio and SUNI@Nio/Col demonstrated a sustained drug release pattern and had uniform nanoscale diameters. The physicochemical characteristics and drug stability of encapsulated sunitinib were improved, thereby enhancing the bioactivity of the drug. The SUNI@Nio SUNI@Nio/COL formulations were shown to trigger apoptosis in lung cancer cell lines (A549) in *in vitro* investigations, which may have been caused by down-regulation or up-regulation of genes associated with apoptosis. Nanotechnology-based intracellular delivery of chemotherapeutic drugs relies heavily on the localization of niosomes within the cells and their interaction with the viable cells. Therapeutic benefits of niosomal formulations may be enhanced by their intercellular localization and prolonged persistence inside cancer cells. This study's findings suggest a promising approach to developing a secure and efficient tailored drug delivery system for the in-vitro treatment of lung cancer.

Data Availability Statement: Data will be available upon request from the corresponding authors.

CRediT authorship contribution statement

Shiva Dehghan: Conceptualization, Investigation. **Amirhossein Naghipour:** Resources. **Fatemeh Zomorodi Anbaji:** Methodology, Software. **Pezhman Golshanrad:** Validation, Data curation. **Hosein Mirazi:** Validation. **Hossein Adelnia:** Writing – review & editing. **Mahdi Bodaghi:** Funding acquisition, Writing – review & editing. **Bahareh Farasati Far:** Conceptualization, Formal analysis, Writing – original draft, Writing – review & editing, Visualization, Supervision, Project administration, Funding acquisition.

Declaration of Competing Interest

The authors declare that they have no known competing financial interests or personal relationships that could have appeared to influence the work reported in this paper.

Data availability

No data was used for the research described in the article.

Appendix A. Supplementary material

Supplementary data to this article can be found online at https://doi.org/10.1016/j.ijpharm.2023.122977.

References

Ahmed, M.M., Anwer, M.K., Fatima, F., Aldawsari, M.F., Alalaiwe, A., Alali, A.S., Alharthi, A.I., Kalam, M.A., 2022. Boosting the anticancer activity of sunitinib malate in breast cancer through lipid polymer hybrid nanoparticles approach. Polymers 14, 2459.

Alharbi, K.S., Shaikh, M.A.J., Afzal, O., Altamimi, A.S.A., Almalki, W.H., Alzarea, S.I., Kazmi, I., Al-Abbasi, F.A., Singh, S.K., Dua, K., 2022. An overview of epithelial growth factor receptor (EGFR) inhibitors in cancer therapy. Chem. Biol. Interact., 110108

Altintas, I., Heukers, R., van der Meel, R., Lacombe, M., Amidi, M., en Henegouwen, P.M. v.B., Hennink, W.E., Schiffelers, R.M., Kok, R.J., 2013. Nanobody-albumin nanoparticles (NANAPs) for the delivery of a multikinase inhibitor 17864 to EGFR overexpressing tumor cells. Journal of Controlled Release 165, 110-118.

Asadi, S., Mortezagholi, B., Hadizadeh, A., Borisov, V., Ansari, M.J., Shaker Majdi, H., Nishonova, A., Adelnia, H., Farasati Far, B., Chaiyasut, C., 2022. Ciprofloxacin-loaded titanium nanotubes coated with chitosan: a promising formulation with sustained release and enhanced antibacterial properties. Pharmaceutics 14, 1359.

Bhia, M., Motallebi, M., Abadi, B., Zarepour, A., Pereira-Silva, M., Saremnejad, F., Santos, A.C., Zarrabi, A., Melero, A., Jafari, S.M., Shakibaei, M., 2021. Naringenin nano-delivery systems and their therapeutic applications. Pharmaceutics 13, 291.

Bianchini, F., De Santis, A., Portioli, E., Krauss, I.R., Battistini, L., Curti, C., Peppicelli, S., Calorini, L., D'Errico, G., Zanardi, F., 2019. Integrin-targeted AmpRGD sunitinib liposomes as integrated antiangiogenic tools. Nanomed. Nanotechnol. Biol. Med. 18, 135–145.

Blumenschein Jr., G.R., Ciuleanu, T., Robert, F., Groen, H.J., Usari, T., Ruiz-Garcia, A., Tye, L., Chao, R.C., Juhasz, E., 2012. Sunitinib plus erlotinib for the treatment of advanced/metastatic non-small-cell lung cancer: a lead-in study. J. Thorac. Oncol. 7, 1406–1416.

Chen, Z., Guo, Y., Zhao, D., Zou, Q., Yu, F., Zhang, L., Xu, L., 2021. Comprehensive Analysis Revealed that CDKN2A is a Biomarker for Immune Infiltrates in Multiple Cancers. Front Cell Dev. Biol. 9, 808208.

Cleland, J.L., Sharma, R., Appiani, S., Prater, J., Spiga, M.G., Culp, D., 2020. Suppression of Murine Choroidal Neovascularization After Systemic Administration of a Targeted Anti-VEGF Therapy. Invest. Ophthalmol. Visual Sci. 61, 3974.

Dolman, M.M., van Dorenmalen, K.M., Pieters, E.H., Sparidans, R.W., Lacombe, M., Szokol, B., Őrfi, L., Kéri, G., Bovenschen, N., Storm, G., 2012. Dendrimer-based macromolecular conjugate for the kidney-directed delivery of a multitargeted sunitinib analogue. Macromol. Biosci. 12, 93–103.

El-Far, S.W., Abo El-Enin, H.A., Abdou, E.M., Nafea, O.E., Abdelmonem, R., 2022. Targeting colorectal cancer cells with niosomes systems loaded with two anticancer drugs models; comparative in vitro and anticancer studies. Pharmaceuticals 15, 816.

Escudero-Ortiz, V., Domínguez-Leñero, V., Catalán-Latorre, A., Rebollo-Liceaga, J., Sureda, M., 2022. Relevance of therapeutic drug monitoring of tyrosine kinase inhibitors in routine clinical practice: a pilot study. Pharmaceutics 14, 1216.

Eshrati Yeganeh, F., Eshrati Yeganeh, A., Fatemizadeh, M., Farasati Far, B., Quazi, S., Safdar, M., 2022. In vitro cytotoxicity and anti-cancer drug release behavior of methionine-coated magnetite nanoparticles as carriers. Med. Oncol. 39, 1–11.

Farasati Far, B., Asadi, S., Naimi-Jamal, M.R., Abdelbasset, W.K., Aghajani Shahrivar, A., 2021. Insights into the interaction of azinphos-methyl with bovine serum albumin: experimental and molecular docking studies. J. Biomol. Struct. Dyn. 1–11.

Farasati Far, B., Bokov, D., Widjaja, G., Setia Budi, H., Kamal Abdelbasset, W., Javanshir, S., Seif, F., Pazoki-Toroudi, H., Dey, S.K., 2022a. Metronidazole, acyclovir and tetrahydrobiopterin may be promising to treat COVID-19 patients, through interaction with interleukin-12. J. Biomol. Struct. Dyn. 1–19.

Farasati Far, B., Naimi-Jamal, M.R., Jahanbakhshi, M., Mohammed, H.T., Altimari, U.S., Ansari, J., 2022b. Poly (3-thienylboronic acid) coated magnetic nanoparticles as a magnetic solid-phase adsorbent for extraction of methamphetamine from urine samples. J. Dispers. Sci. Technol. 1–11.

Farasati Far, B., Naimi-Jamal, M.R., Safaei, M., Zarei, K., Moradi, M., Yazdani Nezhad, H., 2022c. A Review on biomedical application of polysaccharide-based hydrogels with a focus on drug delivery systems. Polymers 14, 5432.
Farmoudeh, A., Akbari, J., Saeedi, M., Ghasemi, M., Asemi, N., Nokhodchi, A., 2020. Methylene blue-loaded niosome: preparation, physicochemical characterization, and in vivo wound healing assessment. Drug Deliv. Transl. Res. 10, 1428–1441.
Foroutan, Z., Afshari, A.R., Sabouri, Z., Mostafapour, A., Far, B.F., Jalili-Nik, M., Darroudi, M., 2022. Plant-based synthesis of cerium oxide nanoparticles as a drug delivery system in improving the anticancer effects of free temozolomide in glioblastoma (U87) cells. Ceram. Int. 48, 30441–30450.
Freitas, L.G.A.d., Isaac, D.L.C., Lima, E.M., Souza, L.G., Abud, M.A., Reis, R.G.d., Tannure, W.T., Ávila, M.P.d., 2018. Retinal changes in rabbit after intravitreal injection of sunitinib encapsulated into solid lipid nanoparticles and polymeric nanocapsules. Arq. Bras. Oftalmol. 81, 408-413.
Fu, Y., Ding, Y., Zhang, L., Zhang, Y., Liu, J., Yu, P., 2021. Poly ethylene glycol (PEG)-Related controllable and sustainable antidiabetic drug delivery systems. Eur. J. Med. Chem. 217, 113372.
Garg, J., Chiu, M.N., Krishnan, S., Tripathi, L.K., Pandit, S., Far, B.F., Jha, N.K., Kesari, K. K., Tripathi, V., Pandey, S., 2022. Applications of lignin nanoparticles for cancer drug delivery: an update. Mater. Lett. 311, 131573.
Gong, P., Wang, Y., Zhang, P., Yang, Z., Deng, W., Sun, Z., Yang, M., Li, X., Ma, G., Deng, G., 2020. Immunocyte membrane-coated nanoparticles for cancer immunotherapy. Cancers 13, 77.
Han, J., Zhang, S., Niu, J., Zhang, C., Dai, W., Wu, Y., Hu, L., 2020. Development of taccalonolide AJ-hydroxypropyl-β-cyclodextrin inclusion complexes for treatment of clear cell renal-cell carcinoma. Molecules 25, 5586.
He, W., Turkeshi, A., Li, X., Zhang, H., 2020. Progress in systemic co-delivery of microRNAs and chemotherapeutics for cancer treatment by using lipid-based nanoparticles. Ther. Deliv. 11, 591–603.
Honarvari, B., Karimifard, S., Akhtari, N., Mehrarya, M., Moghaddam, Z.S., Ansari, M.J., Jalil, A.T., Matencio, A., Trotta, F., Yeganeh, F.E., 2022. Folate-targeted curcumin-loaded niosomes for site-specific delivery in breast cancer treatment: In silico and In vitro study. Molecules 27, 4634.
Jafari, H., Atlasi, Z., Mahdavinia, G.R., Hadifar, S., Sabzi, M., 2021. Magnetic κ-carrageenan/chitosan/montmorillonite nanocomposite hydrogels with controlled sunitinib release. Mater. Sci. Eng. C 124, 112042.
Joseph, J.J., Sangeetha, D., Gomathi, T., 2016. Sunitinib loaded chitosan nanoparticles formulation and its evaluation. Int. J. Biol. Macromol. 82, 952–958.
Karooby, E., Granpayeh, N., 2019. Potential applications of nanoshell bow-tie antennas for biological imaging and hyperthermia therapy. OptEn 58, 065102.
Keutgen, X.M., Ornell, K.J., Vogle, A., Lakiza, O., Williams, J., Miller, P., Mistretta, K.S., Setia, N., Weichselbaum, R.R., Coburn, J.M., 2021. Sunitinib-loaded chondroitin sulfate hydrogels as a novel drug-delivery mechanism for the treatment of pancreatic neuroendocrine tumors. Ann. Surg. Oncol. 28, 8532–8543.
Khan, D.H., Bashir, S., Figueiredo, P., Santos, H.A., Khan, M.I., Peltonen, L., 2019. Process optimization of ecological probe sonication technique for production of rifampicin loaded niosomes. J. Drug Delivery Sci. Technol. 50, 27–33.
Khan, D.H., Bashir, S., Khan, M.I., Figueiredo, P., Santos, H.A., Peltonen, L., 2020. Formulation optimization and in vitro characterization of rifampicin and ceftriaxone dual drug loaded niosomes with high energy probe sonication technique. J. Drug Deliv. Sci. Technol. 58, 101763.
Kishore, R.S.K., Pappenberger, A., Dauphin, I.B., Ross, A., Buergi, B., Staempfli, A., Mahler, H.-C., 2011. Degradation of Polysorbates 20 and 80: studies on thermal autoxidation and hydrolysis. J. Pharm. Sci. 100, 721–731.
Li, H., Zhou, F., Li, L., Zheng, Y., 2016. Design and development of novel MRI compatible zirconium-ruthenium alloys with ultralow magnetic susceptibility. Sci. Rep. 6, 1–10.
Lim, E.-K., Kim, T., Paik, S., Haam, S., Huh, Y.-M., Lee, K., 2015. Nanomaterials for theranostics: recent advances and future challenges. Chem. Rev. 115, 327–394.
Liu, W., Malekahmadi, O., Bagherzadeh, S.A., Ghashang, M., Karimipour, A., Hasani, S., Tlili, I., Goodarzi, M., 2019. A novel comprehensive experimental study concerned graphene oxide nanoparticles dispersed in water: synthesise, characterisation, thermal conductivity measurement and present a new approach of RLSF neural network. ICHMT 109, 104333.
Maitani, Y., Saito, H., Seishi, Y., Iwase, Y., Yamauchi, T., Higashiyama, K., Sugino, T., 2012. A combination of liposomal sunitinib plus liposomal irinotecan and liposome co-loaded with two drugs enhanced antitumor activity in PC12-bearing mouse. J. Drug Target. 20, 873–882.
Malnoë, D., Fardel, O., Le Corre, P., 2022. Involvement of transporters in intestinal drug-drug interactions of oral targeted anticancer drugs assessed by changes in drug absorption time. Pharmaceutics 14, 2493.
Mehrarya, M., Gharehchelou, B., Haghighi Poodeh, S., Jamshidifar, E., Karimifard, S., Farasati Far, B., Akbarzadeh, I., Seifalian, A., 2022. Niosomal formulation for antibacterial applications. J. Drug Target. 30, 476–493.
Mobaraki, F., Momeni, M., Barghbani, M., Far, B.F., Hosseinian, S., Hosseini, S.M., 2022. Extract-mediated biosynthesis and characterization of gold nanoparticles: exploring their protective effect against cyclophosphamide-induced oxidative stress in rat testis. J. Drug Deliv. Sci. Technol. 71, 103306.
Moghtaderi, M., Sedaghatnia, K., Bourbour, M., Fatemizadeh, M., Salehi Moghaddam, Z., Hejabi, F., Heidari, F., Quazi, S., Farasati Far, B., 2022. Niosomes: a novel targeted drug delivery system for cancer. Med. Oncol. 39, 1–22.
Molina, J.R., Yang, P., Cassivi, S.D., Schild, S.E., Adjei, A.A., 2008. Non-small cell lung cancer: epidemiology, risk factors, treatment, and survivorship. Mayo Clin. Proc. 83, 584–594.
Otroj, M., Taymouri, S., Varshosaz, J., Mirian, M., 2020. Preparation and characterization of dry powder containing sunitinib loaded PHBV nanoparticles for enhanced pulmonary delivery. J. Drug Deliv. Sci. Technol. 56, 101570.
Pradhan, M., Srivastava, S., Singh, D., Saraf, S., Saraf, S., Singh, M.R., 2018. Perspectives of lipid-based drug carrier systems for transdermal delivery. Critical Reviews™ in Therapeutic Drug Carrier Systems 35.
Provencio, M., Isla, D., Sánchez, A., Cantos, B., 2011. Inoperable stage III non-small cell lung cancer: Current treatment and role of vinorelbine. Journal of Thoracic Disease; Vol 3, No 3 (September 2011): Journal of Thoracic Disease.
Razmimanesh, F., Sodeifian, G., Sajadian, S.A., 2021. An investigation into Sunitinib malate nanoparticle production by US-RESOLV method: Effect of type of polymer on dissolution rate and particle size distribution. J. Supercrit. Fluids 170, 105163.
Rezaei, T., Rezaei, M., Karimifard, S., Beram, F.M., Dakkali, M.S., Heydari, M., Afshari-Behbahanizadeh, S., Mostafavi, E., Bokov, D.O., Ansari, M.J., 2022. Folic Acid-Decorated pH-Responsive Nanoniosomes With Enhanced Endocytosis for Breast Cancer Therapy. In Vitro Studies. Front, Pharmacol, p. 13.
Saber, M.M., Bahrainian, S., Dinarvand, R., Atyabi, F., 2017. Targeted drug delivery of Sunitinib Malate to tumor blood vessels by cRGD-chiotosan-gold nanoparticles. Int. J. Pharm. 517, 269–278.
Sahrayi, H., Hosseini, E., Karimifard, S., Khayam, N., Meybodi, S.M., Amiri, S., Bourbour, M., Farasati Far, B., Akbarzadeh, I., Bhia, M., 2021. Co-Delivery of Letrozole and cyclophosphamide via folic acid-decorated nanoniosomes for breast cancer therapy: synergic effect, augmentation of cytotoxicity, and apoptosis gene expression. Pharmaceuticals 15, 6.
Sahrayi, H., Hosseini, E., Karimifard, S., Khayam, N., Meybodi, S.M., Amiri, S., Bourbour, M., Farasati Far, B., Akbarzadeh, I., Bhia, M., Hoskins, C., Chaiyasut, C., 2022a. Co-Delivery of letrozole and cyclophosphamide via folic acid-decorated nanoniosomes for breast cancer therapy: synergic effect, augmentation of cytotoxicity, and apoptosis gene expression. Pharmaceuticals 15, 6.
Sahrayi, H., Hosseini, E., Ramazani Saadatabadi, A., Atyabi, S.M., Bakhshandeh, H., Mohamadali, M., Aidun, A., Farasati Far, B., 2022b. Cold atmospheric plasma modification and electrical conductivity induction in gelatin/polyvinylidene fluoride nanofibers for neural tissue engineering. Artif, Organs.
Scrivano, L., Iacopetta, D., Sinicropi, M.S., Saturnino, C., Longo, P., Parisi, O.I., Puoci, F., 2017. Synthesis of sericin-based conjugates by click chemistry: enhancement of sunitinib bioavailability and cell membrane permeation. Drug Deliv. 24, 482–490.
Shaddel, R., Akbari-Alavijeh, S., Cacciotti, I., Yousefi, S., Tomas, M., Capanoglu, E., Tarhan, O., Rashidinejad, A., Rezaei, A., Bhia, M., Jafari, S.M., 2022. Caffeine-loaded nano/micro-carriers: techniques, bioavailability, and applications. Crit. Rev. Food Sci. Nutr. 1–26.
Shahgholi, M., Firouzi, P., Malekahmadi, O., Vakili, S., Karimipour, A., Ghashang, M., Hussain, W., Kareem, H.A., Baghaei, S., 2022a. Fabrication and characterization of nanocrystalline hydroxyapatite reinforced with silica-magnetite nanoparticles with proper thermal conductivity. Mater. Chem. Phys. 289, 126439.
Shahgholi, M., Karimipour, A., Firouzi, P., Malekahmadi, O., Ghashang, M., Saadoon, N., Obaid, N.H., Baghaei, S., 2022b. Fabrication and characterization of synthesized hydroxyapatite/ethanolamine for bone tissue engineering application. Colloids Surf. Physicochem. Eng. Aspects 650, 129591.
Shi, D., Beasock, D., Fessler, A., Szebeni, J., Ljubimova, J.Y., Afonin, K.A., Dobrovolskaia, M.A., 2021. To PEGylate or not to PEGylate: immunological properties of nanomedicine's most popular component, poly (ethylene) glycol and its alternatives. Adv, Drug Del. Rev., p. 114079
Shim, M.K., Yoon, H.Y., Lee, S., Jo, M.K., Park, J., Kim, J.-H., Jeong, S.Y., Kwon, I.C., Kim, K., 2017. Caspase-3/-7-specific metabolic precursor for bioorthogonal tracking of tumor apoptosis. Sci. Rep. 7, 1–15.
Siegel, R., Ma, J., Zou, Z., Jemal, A., 2014. Cancer statistics, 2014. CA Cancer J Clin 64, 9–29.
Speed, B., Bu, H.-Z., Pool, W.F., Peng, G.W., Wu, E.Y., Patyna, S., Bello, C., Kang, P., 2012. Pharmacokinetics, distribution, and metabolism of [14C] sunitinib in rats, monkeys, and humans. Drug Metab. Disposition 40, 539–555.
Stella, G.M., Luisetti, M., Inghilleri, S., Cemmi, F., Scabini, R., Zorzetto, M., Pozzi, E., 2012. Targeting EGFR in non-small-cell lung cancer: Lessons, experiences, strategies. Respir. Med. 106, 173–183.
Streets, J., Bhatt, P., Bhatia, D., Sutariya, V., 2020. Sunitinib-loaded MPEG-PCL micelles for the treatment of age-related macular degeneration. Sci. Pharm. 88, 30.
Tavakoli, S., Puranen, J., Bahrpeyma, S., Lautala, V.E., Karumo, S., Lajunen, T., Del Amo, E.M., Ruponen, M., Urtti, A., 2022. Liposomal sunitinib for ocular drug delivery: A potential treatment for choroidal neovascularization. Int. J. Pharm. 620, 121725.
Torabi, M., Aghanejad, A., Savadi, P., Barzegari, A., Omidi, Y., Barar, J., 2023. Fabrication of mesoporous silica nanoparticles for targeted delivery of sunitinib to ovarian cancer cells. BioImpacts.
Torchilin, V.P., 2005. Recent advances with liposomes as pharmaceutical carriers. Nat. Rev. Drug Discov. 4, 145–160.
Tran, T.H., Poudel, B.K., Kim, J.O., Nguyen, C.N., 2016. Development and Evaluation of Artesunate-Loaded Chitosan-Coated Lipid Nanocapsule as a potential Drug Delivery System Against Breast Cancer. 약품개발연구소 연구업적집 26.
Vázquez, R., Riveiro, M.E., Berenguer-Daize, C., O'kane, A., Gormley, J., Touzelet, O., Rezai, K., Bekradda, M., Ouafik, L.H., 2021. Targeting adrenomedullin in oncology: a feasible strategy with potential as much more than an alternative anti-angiogenic therapy. Front. Oncol. 10, 589218.
Wang, T., Nelson, R.A., Bogardus, A., Grannis Jr., F.W., 2010. Five-year lung cancer survival: which advanced stage nonsmall cell lung cancer patients attain long-term survival? Cancer 116, 1518–1525.
Wang, Y., Tang, X., 2023. Research Progress of Anti-Angiogenic Drugs in First-Line Treatment of Small Cell Lung Cancer. J. Biosciences and Medicines 11, 8–17.
Westerdijk, K., Krens, S.D., van der Graaf, W.T., Mulder, S.F., van Herpen, C.M., Smilde, T., van Erp, N.P., Desar, I.M., 2021. The relationship between sunitinib

exposure and both efficacy and toxicity in real-world patients with renal cell carcinoma and gastrointestinal stromal tumour. Br. J. Clin. Pharmacol. 87, 326–335.
Yang, X., Li, H., Qian, C., Guo, Y., Li, C., Gao, F., Yang, Y., Wang, K., Oupicky, D., Sun, M., 2018. Near-infrared light-activated IR780-loaded liposomes for anti-tumor angiogenesis and Photothermal therapy. Nanomed. Nanotechnol. Biol. Med. 14, 2283–2294.
Yeganeh, F.E., Yeganeh, A.E., Far, B.F., Mansouri, A., Sibuh, B.Z., Krishnan, S., Pandit, S., Alsanie, W.F., Thakur, V.K., Gupta, P.K., 2022a. Synthesis and Characterization of Tetracycline Loaded Methionine-Coated NiFe2O4 Nanoparticles for Anticancer and Antibacterial Applications. Nanomaterials 12, 2286.
Yeganeh, F.E., Yeganeh, A.E., Yousefi, M., Farasati Far, B., Akbarzadeh, I., Bokov, D.O., Raahemifar, K., Soltani, M., 2022b. Formulation and Characterization of Poly (Ethylene Glycol)-Coated Core-Shell Methionine Magnetic Nanoparticles as a Carrier for Naproxen Delivery: Growth Inhibition of Cancer Cells. Cancers (Basel) 14, 1797.
Yongvongsoontorn, N., Chung, J.E., Gao, S.J., Bae, K.H., Yamashita, A., Tan, M.-H., Ying, J.Y., Kurisawa, M., 2019. Carrier-enhanced anticancer efficacy of sunitinib-loaded green tea-based micellar nanocomplex beyond tumor-targeted delivery. ACS Nano 13, 7591–7602.
Zhang, Z., Liu, C., Akakuru, O., Xu, W., Wu, A., Zhang, Y., 2021. ICG and sunitinib-loaded NH2-MOFs for folate-mediated hepatocellular carcinoma dual-modal therapy. Chem. Res. Chin. Univ. 37, 967–974.